energies

MDPI

Article

Innovative Multigeneration System with Heat Exchangers for Harnessing Thermal Energy from Cement Kiln Exhaust Gases

Baby-Jean Robert Mungyeko Bisulandu [1,2,*], Rami Mansouri [3], Marcel Tsimba Mboko [4], Lucien Mbozi Mbozi [4] and Adrian Ilinca [3,*]

[1] Laboratoire de Recherche en Energie Eolienne (LREE), Université du Québec à Rimouski (UQAR), 300 All. des Ursulines, Rimouski, QC G5L 3A1, Canada
[2] Institut de Recherche Futuris—Futuris Research Institute (InReF), OEFC & Institut National du Bâtiment et des Travaux Publics (INBTP), Département de Génie-Rural, Kinshasa B.P. 4731, Democratic Republic of the Congo
[3] Département de Génie Mécanique, École de Technologie Supérieure, Université du Québec, 1100 Rue Notre-Dame Ouest, Montréal, QC H3C 1K3, Canada; rami.mansouri.1@ens.etsmtl.ca
[4] Faculté Polytechnique, Université Président Joseph Kasa-Vubu, Boma B.P. 314, Democratic Republic of the Congo
* Correspondence: baby-jeanrobert.mungyekobisulandu@uqar.ca or jr.bisulandu@gmail.com (B.-J.R.M.B.); adrian.ilinca@etsmtl.ca (A.I.)

Abstract: This article introduces a novel multiple-cycle generation system for efficient heat recovery at high and low temperatures. The system is modeled and optimized using the M2EP analysis method (mass, energy, exergy, and performance) and the particle swarm optimization algorithm. The multigeneration system produces electricity, cold, domestic hot water, and biogas by utilizing Kalina cycles, diffusion–absorption refrigeration machines, and high-performance heat exchangers by harnessing waste heat from cement kiln exhaust gases. The Kalina cycle is employed for electricity generation, wherein the H_2O+NH_3 mixture, heated by hot water, circulates through heat exchangers. Downstream of the Kalina cycle, the refrigeration machine generates cold by evaporating the strong solution of the H_2O+NH_3 mixture. Hydrogen circulates in the diffusion–absorption refrigerator (DAR) circuit, facilitating the exchange between the evaporator and the absorber. The domestic hot water and biogas production systems operate at lower temperatures (around 45 °C). The simulation results for the Kalina cycle indicate an electrical energy production of 2565.03 kW, with a release of usable energy (residual gases) estimated at 7368.20 kW and a thermal efficiency of 22.15%. Exergy destruction is highest at heat exchanger 1, accounting for 26% of the total. A coefficient of performance of 0.268 and an evaporator temperature of 10.57 °C were obtained for the DAR cycle. The absorber contributes the most to energy exchanges, comprising 37% of the entire circuit. Summarizing the potential for valorizing waste heat from cement kilns, this article lays the foundation for future research.

Keywords: multigeneration plant; Kalina cycle; DAR cycle; ammonia–water; waste heat recovery; heating system

Citation: Mungyeko Bisulandu, B.-J.R.; Mansouri, R.; Tsimba Mboko, M.; Mbozi Mbozi, L.; Ilinca, A. Innovative Multigeneration System with Heat Exchangers for Harnessing Thermal Energy from Cement Kiln Exhaust Gases. *Energies* **2024**, *17*, 3041. https://doi.org/10.3390/en17123041

Academic Editor: Francesco Fornarelli

Received: 29 May 2024
Revised: 13 June 2024
Accepted: 18 June 2024
Published: 20 June 2024

1. Introduction

As the energy demand continues to rise, large-scale projects are initiated to capitalize on the residual heat from thermal power installations. The objective is to establish systems capable of recovering energy across various temperature levels at no additional cost. According to data from the International Energy Agency (IEA), global energy demand is projected to increase by 50% in the next decade [1]. The surge in energy consumption is closely tied to the heightened exploitation of natural resources, many of which are non-renewable and contribute to significant environmental imbalances when extracted. Ghasemiasl et al. [2] highlight that climate change, triggered partly by energy consumption,

is expected to escalate with the growth of economic activities and populations, especially in developing countries.

In the face of this energy transition, numerous industrial installations actively explore systems to capture and utilize energy otherwise lost to the environment. They integrate different cycles, such as Kalina, organic Rankine, Brayton, etc., with the residual hot gas exhaust circuit. Taking the cement industry as an example, the gases emitted from chimneys typically have average temperatures of 250 °C, positioning the cement sector as one of the industries with the highest heat loss globally through its exit gases.

This study chose the Kalina and diffusion–absorption refrigeration (DAR) machine cycles due to their established performance and efficiency in industrial energy recovery. The heat exiting the generator of the DAR system is further repurposed for the domestic heating network and biogas production through a digester. The Kalina cycle was patented in the 1980s [3]. It uses a mixture of water and ammonia as the working fluid. The Kalina cycle is capable of operating at temperatures around 400 °C. The increased temperature in the circuit thus allows the fluid to vaporize until optimal vaporization conditions are reached [3]. According to Varma and Srinivas [4] and Júnior et al. [3], the Kalina cycle optimizes the energy efficiency of the conventional Rankine cycle by 20 to 40%. The Kalina cycle can achieve exergy yields of 15 to 18%, relatively high values compared to the organic Rankine cycle, whose exergy yields are between 7 and 10%. Cheng et al. [5] state that the Kalina cycle is a promising technology for converting low-grade heat into electricity. Hossain et al. [6] note that the Kalina cycle is increasingly used in high-temperature applications (where the working fluid sometimes reaches 500 °C at the turbine inlet). Figure 1 describes the application of the Kalina cycle dedicated to electricity production.

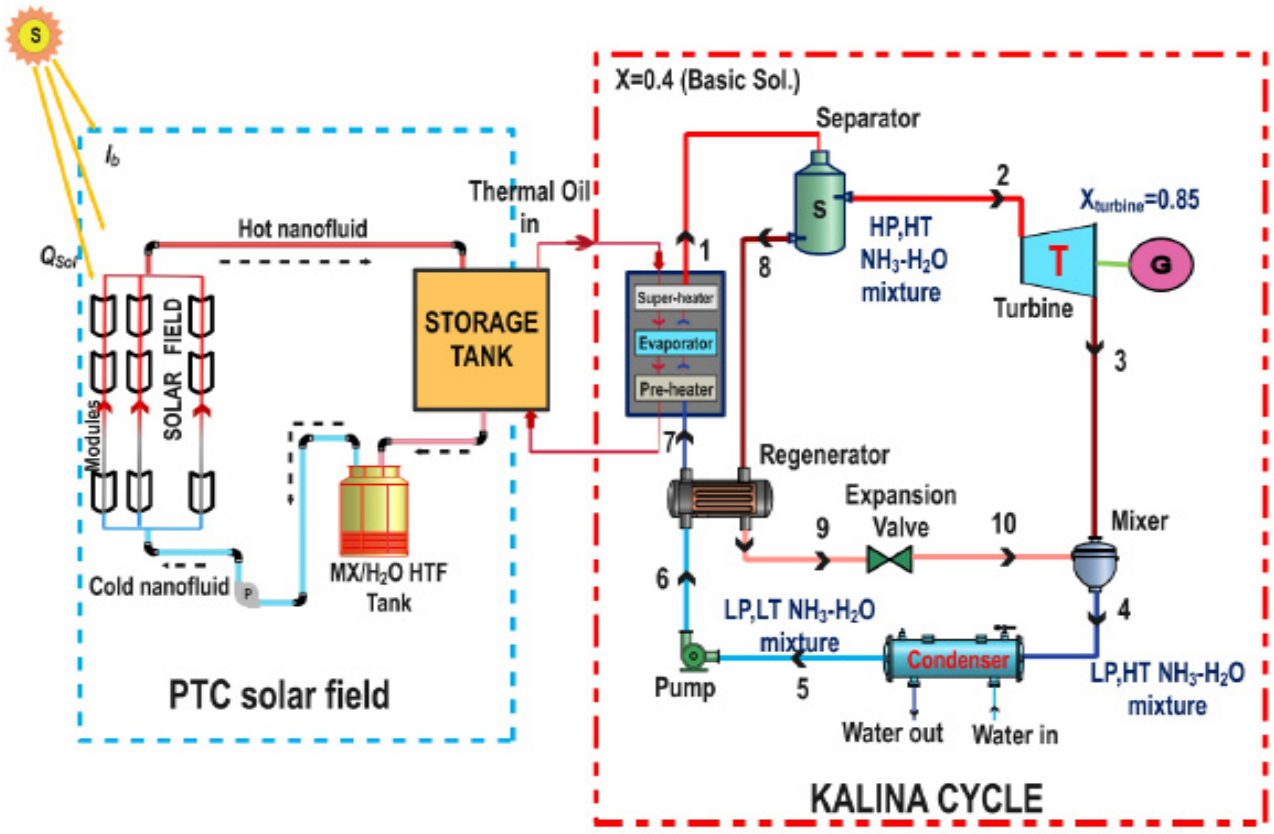

Figure 1. Representation of Parabolic Trough Collector (PTC) solar field and Kalina cycle integration [7].

Numerous works in the literature deal with waste heat recovery using the Kalina cycle. Da Costa Horta et al. [8] were interested in studying electricity cogeneration in the cement plant to establish a comparison based on the operating and performance characteristics of

the two Kalina cycles studied. The results show that one of the Kalina cycles can produce acceptable electrical power.

Ma et al. [9] investigated a flue gas waste heat recovery system consisting of a flue gas heat transfer system and air heat transfer systems. The main goal was to improve system performance. Zhao et al. [10] were interested in the recovery of residual heat from the silicon production system for the hybrid system, that is, the production of electricity and heat necessary for the pyrolysis of tires. To achieve their objectives, the authors considered the hybrid system's thermodynamic and techno-economic aspects. This study found energy and exergy efficiencies of 64.14% and 72.13%, respectively. Cao et al. [11] focused on studying how to valorize waste heat from gas turbine exhaust gases in a hybrid supercritical–transcritical carbon dioxide (CO_2) waste heat recovery system, where the inlet pressure of the turbine and mass flow played an important role in achieving system performance. Zhang et al. [12] proposed a system for recovering residual heat from combustion gases integrated into the bypass duct and the exterior primary air preheater of a bitumen-fired power plant with the aim of limiting heat losses due to the mixture of cold air with heated primary air. The system is optimized using the thermo- and techno-economic analysis models of the waste heat recovery system.

The results show that the exergy efficiency of the waste heat recovery system can reach 49.8%. Fu et al. [13], in their work on the thermo-economic analysis of a new cogeneration system for the cascade recovery of residual heat from combustion gases, showed that it was possible to valorize low-quality residual heat at both an absorption refrigeration cycle (ARC) and an organic Rankine cycle (ORC). The energy efficiency found is 54.84%. The energy production is 1866.10 kW for an ORC evaporation temperature of 145 °C. The exergy efficiency amounts to 34.57%, with an available energy of 1233.3 kW. Feng et al. [14] designed a waste heat recovery system from flue gas from low-temperature sintering cooling in an annular cooler for power generation to improve the thermal recovery and utilization efficiency of the residual heat from sintering and the organic Rankine cycle. The working fluid used is R600a. The results show that the net power output of the system increases with increasing evaporation temperature. Wang et al. [15] analyzed and optimized an organic Rankine flash cycle dedicated to low-temperature heat recovery using the 3E (energy, exergy, and economic) analysis method and the swarm optimization algorithm of particles. They used five organic fluids and three typical heat source conditions to completely understand and control the thermo-economic characteristics of the system. Benvenuto et al. [16] explored the possibilities of recovering waste heat from diesel engine exhaust gases to meet energy needs. Among the proposed solutions is using either a steam turbine and a gas turbine or simply a steam turbine for electricity production. The results of the study showed that the gas turbine increases the system's efficiency and reduces the steam turbine's power. Liang et al. [17] were interested in the valorization of waste heat from the cooling of supercritical CO_2 and combustion gases to improve the efficiency of electricity production based on the Brayton cycle. The authors recommend integrating the organic Rankine cycle and the $LiBr/H_2O$ absorption refrigeration cycle, aiming to better waste heat recovery performance. Zhu et al. [18] explored the possibility of producing electricity from liquefied natural gas using thermoelectric generators (TEG). This involves the recovery of cold energy from the liquefaction of natural gas. To avoid the risk of icing, the cryogenic thermoelectric generator uses natural gas vapor on the hot side of the TEG. A maximum power output of 593.94 W was achieved.

Absorption refrigeration machines are a viable alternative for harnessing low-quality waste heat at lower temperatures. The concept of the absorption machine dates to 1859, stemming from the pioneering work of Ferdinand Carré, who patented the technology in the same year. In contemporary times, the global push for energy transition, a policy aimed at promoting the adoption of environmentally friendly and less polluting green energies, significantly advocates for the refrigeration sector to embrace sustainable systems, mainly through the widespread adoption of absorption refrigeration machines. As Asfand and Bourouis [14] highlighted, the global community grapples with an impending energy

shortage, emphasizing the growing significance of absorption refrigeration systems. Working fluids are environmentally friendly and have low ODP (ozone depletion potential), encouraging many industrialists to opt for Kalina cycle systems, with ongoing research to achieve economically viable and efficient thermal systems. Efforts in this direction involve optimizing the selection and sizing of essential system components, including the absorber, generator (or boiler), energy source, condenser, and evaporator, and potentially incorporating heat exchangers and pumps. Research also explores integrating different technologies, such as combining compression and absorption machines or leveraging multiple energy sources. Notably, the development of absorption machines is gaining increasing importance, particularly in applications related to air conditioning and preservation [19–25]. Figure 2 illustrates a schematic diagram of the DAR cycle, featuring a generator, rectifier, condenser, and evaporator coupled with a gas heat exchanger, absorber, reservoir, and solution heat exchanger.

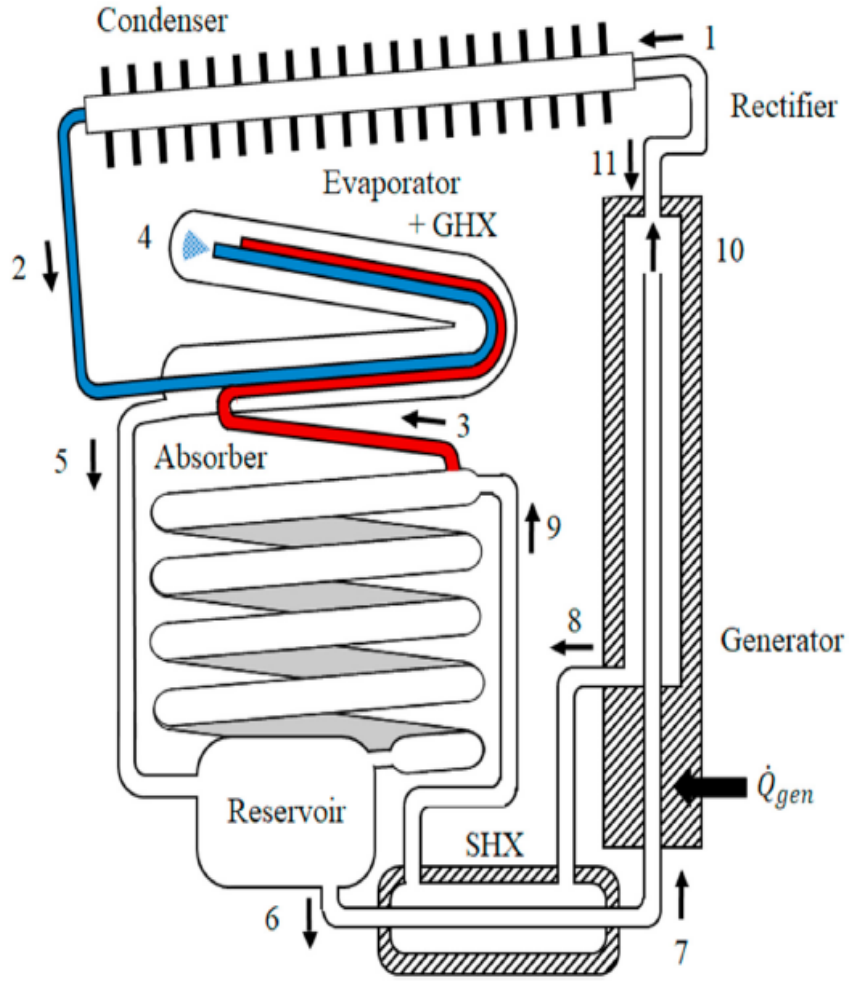

Figure 2. Schematic diagram of the DAR [26].

Numerous studies in the literature delve into diffusion–absorption refrigeration machines, exploring their utilization with diverse energy sources. For instance, Dhindsa [27] evaluated energy sources that can power thermochemical absorption solar hybrid refrigeration systems. This study shows that the so-called renewable sources can be used to operate such types of systems. Alcantara et al. [28] developed a mathematical model to simulate the behavior of absorption coolers with $NH_3/LiNO_3$ working fluid. An additional component known as a "rectifier" is essential to purify the refrigerant before entering the condenser. Given the volatility of the absorbent (water), it evaporates alongside ammonia (refrigerant).

Without the rectifier, the water condenses and accumulates inside the evaporator, leading to diminished performance.

A multigeneration cycle was proposed by Fouda et al. [29]. This system comprises several subsystems, encompassing the absorption refrigeration cycle, the organic Rankine cycle, and a proton exchange membrane electrolyzer. Almohammadi et al. [30] also studied a multigeneration system using solar energy as an energy source. The system includes an organic Rankin cycle, a water desalination system by humidification and dehumidification, a desiccant cooling system to produce electrical energy, and a water desalination system and air conditioning. The objective is to compensate for the energy deficit in certain gulf countries.

The novelty of this manuscript lies in the fact that the multiple-cycle generation system developed here is designed for heat recovery at both high and low temperatures at a lower cost. The Kalina cycle system proposed in this work is more energy efficient and improves the power generation performance by more than 50% compared to the conventional Kalina cycle. Although powered by an energy source with a relatively low temperature, the DAR system produced acceptable efficiency and a cooling capacity of 6.77 MW. Also, this study went far by exploiting the residual heat of the outlet gases at the level of the bubble pump, which had been used to heat the H_2O-NH_3 solution in the DAR cycle. A heat exchanger uses this thermal energy to heat water for domestic use. The energy contained in the gases released from this heat exchanger is used again to produce biogas.

2. Materials and Methods

2.1. System Description

The proposed multigeneration system outlined in this article encompasses four primary components: electricity production, cold generation, heat production (for domestic hot water), and biogas production. The system is equipped with a heat recovery mechanism within the cyclone tower and the clinker cooling stack of a rotary cement kiln, both exhibiting temperatures exceeding 150 °C. The residual gases heat water through heat exchangers integrated into the circuit. The heated water is directed to the exchangers through which the refrigerant fluids (specifically, the H_2O+NH_3 mixture) pass. The electricity production circuit operates based on the Kalina cycle (Figure 3) following the following steps:

1. Pump 1 is responsible for drawing the water–ammonia mixture under atmospheric conditions and transferring it to a preheater.
2. Once preheated, the mixture proceeds to an evaporator, undergoing evaporation. The resulting steam is then directed to the first superheater for additional heating.
3. The superheated mixture enters the high-pressure turbine, where thermal energy is converted into kinetic energy at the turbine shaft.
4. After expansion in the high-pressure turbine, the steam passes through the second superheater before entering the medium-pressure turbine. This process converts thermal energy into kinetic energy, driving an electric generator.
5. Following expansion in the medium-pressure turbine, the steam moves on to the low-pressure turbine, further expanding and contributing to additional electrical energy generation through coupling with the generator.
6. Maintaining a constant concentration, the steam passes through a heat exchanger or recuperator, preheating the mixture from the pump.
7. Exiting the recuperator, the mixture then enters the condenser. The pump then draws in the condensed mixture to repeat the cycle.

This Kalina cycle configuration facilitates the efficient conversion of thermal energy into electrical energy, forming a vital component of the multigeneration system's overall functionality.

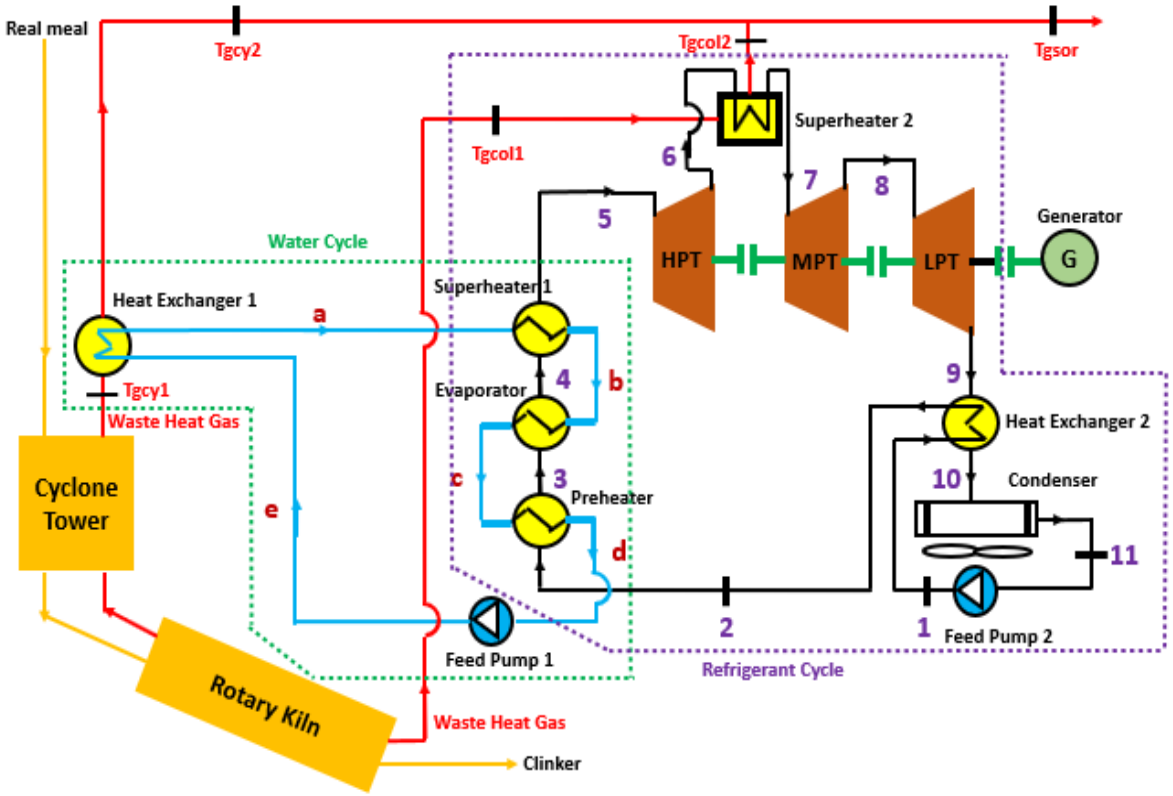

Figure 3. Diagram of Kalina cycle system.

The gases emanating from various heat exchangers (gas–water) retain a significant amount of recoverable energy, leading to the integration of the DAR cycle into the system. The DAR system employed in this article follows the configuration introduced in the work of Mazouz et al. [31]. This DAR system comprises a rectifier, a condenser, an absorber, an evaporator, and a generator designed as two externally heated coaxial tubes. The inner tube functions as the bubble pump, receiving heat indirectly through the solution flowing in the annular space, acting as a boiler. The heat $\dot{Q}_{gen}$ supplied to the generator facilitates degassing a fraction of the ammonia in the rich solution from the absorber. The resulting ammonia vapors are subsequently purified in the rectifier through partial condensation of the remaining water vapors, with the heat rejected in the rectifier denoted as $\dot{Q}_{rec}$. The nearly pure ammonia then condenses in the condenser, releasing heat $\dot{Q}_{cond}$ to the environment. The condensate undergoes sub-cooling in the gas heat exchanger before evaporating at low temperature in the evaporator, producing useful cooling capacity $\dot{Q}_{evap}$. The gas mixture exiting the evaporator is directed to the bottom of the absorber, where it flows upward in a counter-current manner to the weak solution coming from the generator, fed at its top. The exothermic absorption of ammonia in the aqueous solution is accompanied by the rejection of heat $\dot{Q}_{abs}$ to the ambient [31]. Thus, $\dot{Q}_{gen}$ represents the energy derived from the hot gases in the gas–water exchangers. Upon exiting the generator, the gases retain sensible energy, which is utilized in two configurations: the production of domestic hot water through a heat exchanger and the production of biogas. In the latter, the residual gases heat the walls of the gasifier, accelerating the decomposition of the organic waste inside the enclosure and facilitating biogas production. Figure 4 illustrates the second part of the multigeneration system under study in this article.

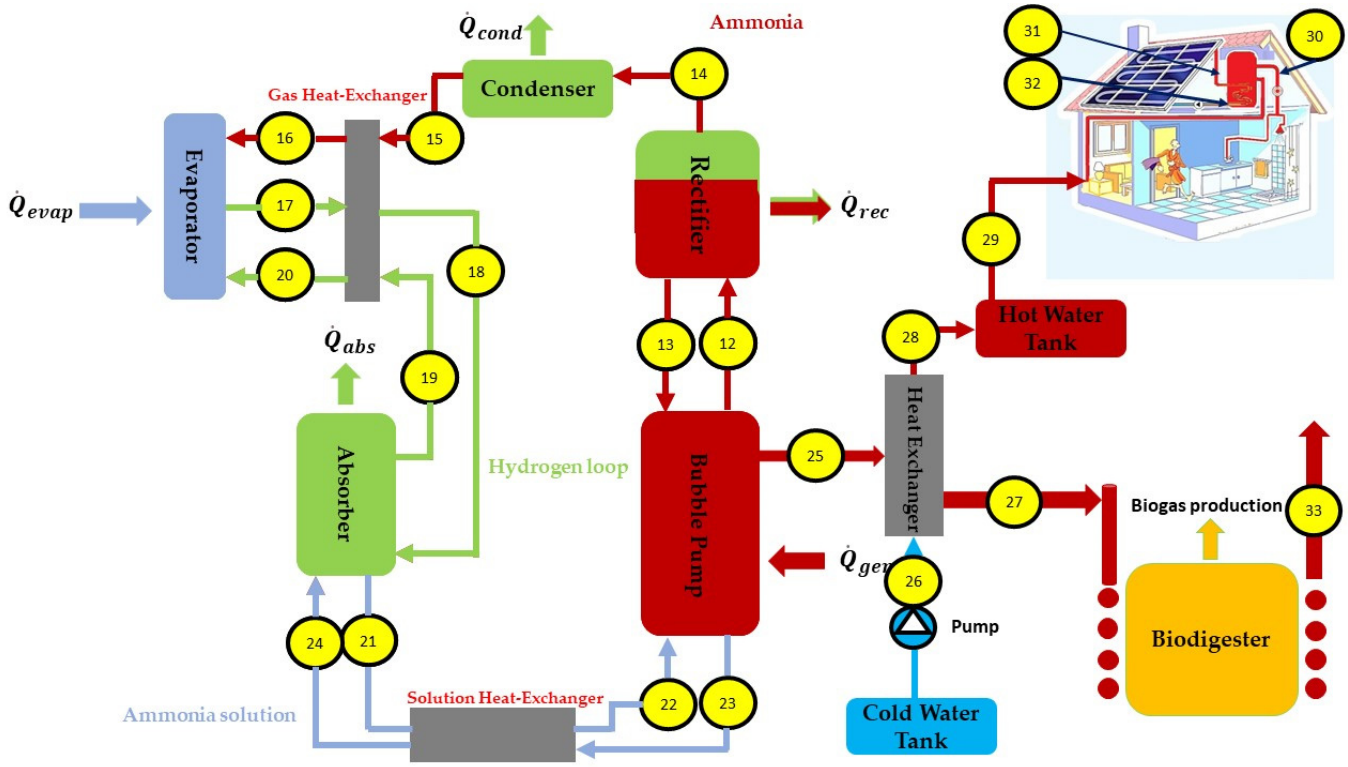

Figure 4. Diagram of DAR cycle, domestic hot water, and biogas production systems.

2.2. Absorption Working Fluids Selection

Selecting the appropriate working fluid or solution is crucial in operating a heat recovery system. The thermophysical properties of the chosen working fluid significantly influence the system's performance. Factors to consider include the rate of evaporation at the saturation point, safety considerations (harmfulness in case of accidents or leaks in the installation), and global warming potential (GWP) values. Different fluids exhibit varying characteristics in evaporation rates, safety profiles, and environmental impact, making the choice of the working fluid a pivotal aspect of system design and operation.

Typically, the thermodynamic properties of working fluids are presented in diagrams. According to Cefarin [32], critical thermodynamic properties crucial for designing an absorption system include pressure, temperature, mass fraction, enthalpy, specific volume, and entropy. Various studies have employed the water–ammonia mixture in the literature due to its efficacy in the absorption machine cycle. This mixture is recognized for harnessing heat sources at low temperatures (80–200 °C). In the current study, the ternary water–ammonia–hydrogen mixture is utilized, both in the Kalina and the DAR machine cycles. This choice is motivated by the mixture's performance characteristics, particularly its suitability for exploiting low-temperature heat sources. The curves in Figure 5 were drawn based on the information and data from the work of Vijayaraghavan [33].

2.3. Benefits, Safety Risks, and Remedies of Using Ammonia

Ammonia is a flammable product with an auto-ignition temperature of around 651 °C and an octane number of 130 [34], higher than methane and propane. According to Shanmugam and Mital [35], anhydrous ammonia is the most used in large refrigeration systems because it has better physical properties than the competing refrigerants (3 to 10% more efficient). Ammonia is known to have an ozone depletion potential (ODP) and global warming potential (GWP) of zero [35–38]. For Yamamoto et al. [36], the water–ammonia mixture is the natural working fluid par excellence for absorption refrigeration systems and allows a wide range of operating temperatures. Because of the above, ammonia is considered a natural refrigerant that decomposes easily in the environment. Although

ammonia has energy and environmental benefits, it is hazardous to human life. It can cause burns to the skin and eyes and lung problems, and can be fatal, especially at high concentrations (about 15 to 28 percent of air volume). Ammonia can explode if released into an enclosed space where there is an ignition source or if a container containing ammonia is exposed to sufficient heat [35,39]. Hence, there is a need to adequately protect and always inspect ammonia pipes to avoid leaks that could endanger the lives of personnel and even cause a material accident. According to Shanmugam and Mital [35], in the United States of America, ammonia refrigeration systems containing 4536 kg or more of ammonia are subject to the OSHA Process Safety Management (PSM) standard and management program EPA Risk Assessment (RMP).

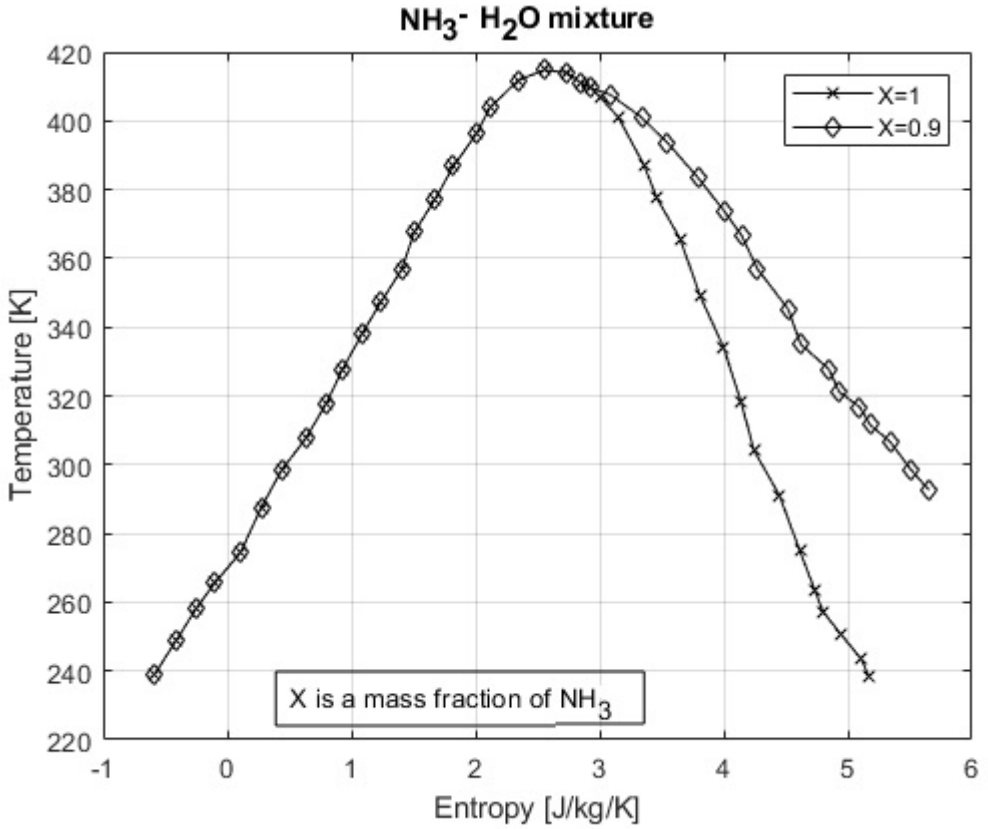

Figure 5. T-s diagram of ammonia–water mixture.

3. Modeling of the Multigeneration System

This section presents the physical modeling of different systems constituting the overall system. Firstly, the hypotheses used are presented, then the mathematical equations reflecting the operation of these systems are modeled. Finally, the mixing model of the fluids used is presented.

3.1. Main Assumptions

In this article, the following hypotheses have been adopted:

For the Kalina Cycle, additional details are available in a previous publication [40]:

- The system is in a state of equilibrium, with no consideration given to kinetic or potential energies.
  - Pump 1 operates under ambient room temperature conditions.
  - Ammonia and water mixing takes place at room temperature.
- Heat losses from both the power cycle components and the surrounding environment are disregarded.

- A pinch point of 10 K is assumed for the superheaters, while a fixed efficiency of 60% is assigned to the remaining exchangers.
- Both Pump 1 and Pump 2 draw fluids at a temperature of 30 °C.
- At the inlet, the concentration is 88% for NH_3 (ammonia) and 12% for water.

For the DAR Cycle:

- Temperature variations directly influence changes in the NH_3 concentration.
- The temperature at points 24 and 15 is equal (T24 = T15).

3.2. Mass, Energy, and Exergy Analysis

The thermodynamic equations characterizing the multigeneration system are given in the following tables (Tables 1 and 2). These equations are based on the two main laws of thermodynamics.

3.3. Thermodynamic Modeling of Refrigerant Mixing

The isentropic or energy efficiencies, the energy and exergy balance, and the irreversibility of each component play a significant role in the modeling process of the present multigeneration system (especially Kalina and DAR). Given that the concentration of ammonia in the mixture greatly influences the cycle's performance, this article will use the information in the work of Mungyeko Bisulandu et al. [40], which states that the enthalpy at each cycle point is the weighted sum of the enthalpies of each species in the refrigerant mixture.

Table 1. Mass, energy, and exergy balance of multigeneration system.

Components	Mass Balance Equations	Energy Balance Equations	Exergy Balance Equations
KALINA CYCLE			
Preheater	$\dot{m}_2 = \dot{m}_3$ AND $\dot{m}_c = \dot{m}_d$	$\dot{Q}_{preh} = \dot{m}_1(h_3 - h_2) = \dot{m}_a(h_d - h_c)$	$\dot{E}x_2 + \dot{E}x_c = \dot{E}x_3 + \dot{E}x_d + \dot{E}x^D_{Preh}$
Evaporator	$\dot{m}_3 = \dot{m}_4$ AND $\dot{m}_c = \dot{m}_b$	$\dot{Q}_{evap} = \dot{m}_1(h_4 - h_3) = \dot{m}_a(h_c - h_b)$	$\dot{E}x_3 + \dot{E}x_b = \dot{E}x_4 + \dot{E}x_c + \dot{E}x^D_{Evap}$
Superheater 1	$\dot{m}_4 = \dot{m}_5$ AND $\dot{m}_a = \dot{m}_b$	$\dot{Q}_{superh1} = \dot{m}_1(h_5 - h_4) = \dot{m}_a(h_b - h_a)$	$\dot{E}x_4 + \dot{E}x_a = \dot{E}x_5 + \dot{E}x_b + \dot{E}x^D_{Superh1}$
Superheater 2	$\dot{m}_6 = \dot{m}_7$ AND $\dot{m}_{gcol1} = \dot{m}_{gcol2}$	$\dot{Q}_{superh2} = \dot{m}_1(h_6 - h_7) = \dot{m}_{gcol}(h_{gcol2} - h_{gcol1})$	$\dot{E}x_6 + \dot{E}x_{gcol1} = \dot{E}x_7 + \dot{E}x_{gcol2} + \dot{E}x^D_{Superh2}$
HPT	$\dot{m}_5 = \dot{m}_6$	$w_{HPT} = h_5 - h_6$	$\dot{E}x_5 = \dot{E}x_6 + \dot{w}_{HPT} + \dot{E}x^D_{HPT}$
LPT	$\dot{m}_8 = \dot{m}_9$	$w_{LPT} = h_8 - h_9$	$\dot{E}x_8 = \dot{E}x_9 + \dot{w}_{LPT} + \dot{E}x^D_{LPT}$
MPT	$\dot{m}_7 = \dot{m}_8$	$w_{MPT} = h_7 - h_8$	$\dot{E}x_7 = \dot{E}x_8 + \dot{w}_{MPT} + \dot{E}x^D_{MPT}$
Heat Exchanger 2	$\dot{m}_9 = \dot{m}_{10}$ AND $\dot{m}_1 = \dot{m}_2$	$\dot{Q}_{HEX2} = \dot{m}_9(h_9 - h_{10}) = \dot{m}_1(h_2 - h_1)$	$\dot{E}x_9 + \dot{E}x_1 = \dot{E}x_{10} + \dot{E}x_2 + \dot{E}x^D_{HEX2}$
Condenser	$\dot{m}_{10} = \dot{m}_{11}$	$\dot{Q}_{cond} = \dot{m}_{10}(h_{10} - h_{11})$	$\dot{E}x_{10} = \dot{E}x_{11} + \dot{E}x^D_{Cond}$
Feed Pump 1	$\dot{m}_a = \dot{m}_e = \dot{m}_d$	$w_{pump1} = h_1 - h_{11}$	$\dot{E}x_{11} = \dot{E}x_1 - \dot{w}_{Pump2} + \dot{E}x^D_{Pump2}$
Feed Pump 2	$\dot{m}_{11} = \dot{m}_1$	$w_{pump2} = h_e - h_d$	$\dot{E}x_d = \dot{E}x_e - \dot{w}_{Pump1} + \dot{E}x^D_{Pump1}$
Heat Exchanger 1	$\dot{m}_{gcy1} = \dot{m}_{gcy2}$ AND $\dot{m}_a = \dot{m}_e$	$\dot{Q}_{HEX1} = \dot{m}_{gcy}(h_{gcy2} - h_{gcy1}) = \dot{m}_a(h_a - h_e)$	$\dot{E}x_{gcy1} + \dot{E}x_e = \dot{E}x_{gcy2} + \dot{E}x_a + \dot{E}x^D_{HEX1}$
DAR SYSTEM			
Bubble Pump	$\dot{m}_{22} + \dot{m}_{13} = \dot{m}_{12} + \dot{m}_{23}$	$\dot{Q}_{gen} = \dot{m}_{22}h_{22} + \dot{m}_{13}h_{13} - \dot{m}_{12}h_{12} - \dot{m}_{23}h_{23}$	$\dot{E}x_{13} + \dot{E}x_{22} = \dot{E}x_{12} + \dot{E}x_{23} + \dot{E}x^D_{gen}$
Rectifier	$\dot{m}_{12} = \dot{m}_{13} + \dot{m}_{14}$	$\dot{Q}_{rec} = \dot{m}_{12}h_{12} - \dot{m}_{13}h_{13} - \dot{m}_{14}h_{14}$	$\dot{E}x_{14} + \dot{E}x_{13} = \dot{E}x_{12} + \dot{E}x^D_{rec}$
Condenser	$\dot{m}_{14} = \dot{m}_{15}$	$\dot{Q}_{cond} = \dot{m}_{14}(h_{15} - h_{14})$	$\dot{E}x_{15} = \dot{E}x_{14} + \dot{E}x^D_{Cond}$
GHX Exchanger	$\dot{m}_{15} = \dot{m}_{16}$ $\dot{m}_{17} = \dot{m}_{18}$ $\dot{m}_{19} = \dot{m}_{20}$	$\dot{Q}_{GHX} = \dot{m}_{15}(h_{16} - h_{15}) = \dot{m}_{17}(h_{18} - h_{17}) = \dot{m}_{19}(h_{20} - h_{19})$	$\dot{E}x_{15} + \dot{E}x_{17} + \dot{E}x_{19} = \dot{E}x_{16} + \dot{E}x_{18} + \dot{E}x_{20} + \dot{E}x^D_{GHX}$
Evaporator	$\dot{m}_{16} + \dot{m}_{20} = \dot{m}_{17}$	$\dot{Q}_{evap} = \dot{m}_{17}h_{17} - \dot{m}_{16}h_{16} - \dot{m}_{20}h_{20}$	$\dot{E}x_{16} + \dot{E}x_{20} = \dot{E}x_{17} + \dot{E}x^D_{evap}$
Absorber	$\dot{m}_{18} + \dot{m}_{24} = \dot{m}_{19} + \dot{m}_{21}$	$\dot{Q}_{abs} = \dot{m}_{18}h_{18} + \dot{m}_{24}h_{24} - \dot{m}_{19}h_{19} - \dot{m}_{21}h_{21}$	$\dot{E}x_{24} + \dot{E}x_{18} = \dot{E}x_{21} + \dot{E}x_{19} + \dot{E}x^D_{abs}$
SHX Exchanger	$\dot{m}_{21} = \dot{m}_{22}$ AND $\dot{m}_{23} = \dot{m}_{24}$	$\dot{Q}_{SHX} = \dot{m}_{21}(h_{22} - h_{21}) = \dot{m}_{23}(h_{24} - h_{23})$	$\dot{E}x_{23} + \dot{E}x_{21} = \dot{E}x_{24} + \dot{E}x_{22} + \dot{E}x^D_{SHX}$

Table 1. *Cont.*

Components	Mass Balance Equations	Energy Balance Equations	Exergy Balance Equations
DOMESTIC HEATING NETWORK			
Heat Exchanger	$\dot{m}_{25} = \dot{m}_{27}$ AND $\dot{m}_{26} = \dot{m}_{28}$	$\dot{Q}_{HExW} = \dot{m}_{25}(h_{27} - h_{25}) = \dot{m}_{26}(h_{28} - h_{26})$	$\dot{Ex}_{25} + \dot{Ex}_{26} = \dot{Ex}_{27} + \dot{Ex}_{28} + \dot{Ex}^{D}_{HExW}$
Hot Water Tank	$\dot{m}_{28} = \dot{m}_{29}$	$\dot{Q}_{HWT} = \dot{m}_{28}(h_{29} - h_{28})$	$\dot{Ex}_{28} = \dot{Ex}_{29} + \dot{Ex}^{D}_{HWT}$
Hot Water Tank 2	$\dot{m}_{29} = \dot{m}_{30}$ AND $\dot{m}_{31} = \dot{m}_{32}$	$\dot{Q}_{HWT2} = \dot{m}_{29}(h_{30} - h_{29}) - \dot{m}_{31}(h_{32} - h_{31})$	$\dot{Ex}_{29} + \dot{Ex}_{31} = \dot{Ex}_{30} + \dot{Ex}_{32} + \dot{Ex}^{D}_{HWT2}$
BIODIGESTER			
Biogas Production	$\dot{m}_{27} = \dot{m}_{33}$	$\dot{Q}_{BGP} = \dot{m}_{27}(h_{33} - h_{27}) + \dot{m}_{waste}h_{waste}$	$\dot{Ex}_{27} = \dot{Ex}_{33} + \dot{Ex}^{D}_{BGP}$

Table 2. Performance parameters of multigeneration system.

Components	Performance Parameters
KALINA CYCLE	
Net work	$\dot{w}_{net} = \dot{w}_T - \dot{w}_P$
Energy efficiency	$\eta_{Energy} = \frac{\dot{w}_{Net}}{\dot{Q}_{HR} - \dot{Q}_{Rec}}$
Exergy efficiency	$\eta_{Exergy} = \frac{\dot{w}_{Net}}{\dot{E}x_{In}^{HR}}$
DAR SYSTEM	
COP	$COP = \frac{Q_{evap}}{Q_{gen}}$
Temperature of evaporator	$T_{evap} = (1 - \varepsilon)T_{amb} + \varepsilon T_{16}$ [1]
Net cooling capacity	$\dot{Q}_{evap} = \dot{m}_{17}h_{17} - \dot{m}_{16}h_{16} - \dot{m}_{20}h_{20}$
DOMESTIC HEATING NETWORK	
Thermal power	$\dot{Q}_{DHN} = \dot{m}_{28}h_{28+}\dot{m}_{27}h_{27} - (\dot{m}_{25}h_{25} + \dot{m}_{26}h_{26})$
Energy efficiency	$\eta_{Energy} = \frac{T_{rej2} - T_{rej3}}{T_{rej2}}$
BIODIGESTER	
Thermal power	$T_{waste,2} = \frac{\dot{m}_{27} \times Cp_{27} \times T_{27}}{\dot{m}_{waste} \times Cp_{waste}} + T_{waste,1}$
Energy efficiency	$\eta_{Energy} = \frac{T_{rej3} - T_{waste,2}}{T_{rej3}}$

[1] formula established based on the following relationship: $\varepsilon_{vap} = \frac{T_{amb} - T_{evap}}{T_{amb} - T_{16}}$.

4. Model Validation

The original contribution of this work addresses integrating multiple energy recovery and generation techniques. Therefore, the validation of this model is performed separately for electricity production, cold production, and heat production.

4.1. Kalina Cycle System Results Validation

Our previous work [40] provides details on validating electricity production. The comparison parameters are thermal efficiency, operating temperature, exergy efficiency, and electrical power. The analyses show significant similarities with the work of Júnior et al. [3]. Table 3 presents simulation errors compared between Júnior et al. [3] and this model. Since the errors found are minimal, this model is valid and reliable.

Table 3. Comparison of results and simulation error calculation.

Parameters	Júnior et al. [3]	Present Model	Error %
Temperature [°C]	390	300	23.08
Exergetical Efficiency [%]	47.8	40.35	15.59
Thermal Efficiency [%]	23.3	22.15	4.94
Net Electrical Power [kWe]	2429.056	2565.03	5.60

The significant differences in temperatures between the works of Júnior et al. [3] and the present model are because the models have different types of cycles and whose energy sources (energy recovery in the gases leaving the kiln) are found in different places in the circuit of the rotary kiln. The error of 23% is due to the different designs adopted in the models of the heat recovery exchangers and the location of the energy recovery exchanger in the gas circuit leaving the cement production rotary kiln.

4.2. Comparison of DAR Cycle System Results with Similar Literature Applications

This article's results were compared to similar works in the literature to validate the DAR cycle model. The comparison concerns the installation's performance and operating

parameters (input and output). Table 4 compares the operating parameters of this simulation with the ones of Rattner and Garimella [41,42]. The two have very similar operating parameters. As input parameters, the works found in the literature use the values of 24 °C and 130 °C, respectively, as the ambient temperature and exchange temperature at the generator level. In our simulation, we used 30 °C and 109 °C as the ambient and exchange temperatures at the generator. As for the working pressure, they use a value of 11.5 bars, slightly lower than that of the model presented, which amounts to 20 bars. A difference of approximately 8.5 bars emerges. Regarding the performance parameters, the two works have almost the same COP value, i.e., 0.26, with a difference of 0.0082.

Table 4. Comparison between the results of the DAR cycle of this model and those found in the literature.

Parameters	Rattner and Garimella [41,42]	Present Model	Gap
Type of refrigeration machine	DAR	DAR	-
Ambient temperature	24 °C	30 °C	+6 °C
Exchange temperature at the generator	130 °C	109 °C	−21 °C
Pressure	11.5 bars	20 bars	+8.5 bars
Working fluids	NH_3-NaSCN-He	NH_3-H_2O-H_2	-
COP found	26%	26.82%	+0.82%

Our simulations agree with Rattner and Garimella's data [41,42]. There is no significant difference between the literature data and actual performance, including ambient temperature, exchange temperature at the generator, pressure, and COP. The analyses and comparisons above allow us to conclude that this model is valid and reliable.

5. Results and Discussion

5.1. Data of Study

The data and operating conditions from an existing cement kiln located in Congo-Kinshasa facilitate the development and simulation of the multigeneration system. These technical and industrial data are used to simulate the system studied. Detailed information on the operating parameters of the Kalina cycle is given in [43], and that of the DAR cycle is given in Table 5.

Table 5. Operating parameters of the DAR cycle, domestic hot water, and biogas production system.

Operating Parameters	Values
Gas temperature at generator inlet ($T_{gas\cdot gen}$)	109.5 °C
The mass flow rate of working fluid (H_2O+NH_3)	22.32 kg/s
The mass flow rate of H_2	14.83 kg/s
Ambient temperature	30 °C
Rectifier pinch-point temperature difference	10 °C
The efficiency of the absorber	80% [44]
The efficiency of evaporator	80% [1]
The efficiency of heat exchangers	70% [45]
The concentration of NH_3 in the mixture at the pump discharge	30% [43]
Evaporator pinch-point temperature difference	10 °C [46]
SHX efficiency	70% [45]
The mass flow rate of waste (biomass)	500 kg/s
Average waste temperature	20 °C
Lower calorific Value	17.2 MJ/kg

[1] value estimated based on the efficiency of the absorber which is 80%.

5.2. Kalina Cycle System

5.2.1. Thermodynamic Performance

This study comprehensively analyses the thermodynamic performances of the Kalina cycle designed explicitly for electricity production. The results of this analysis are briefly presented in Table 6. The results obtained in this part concern the energy modeling of the Kalina cycle (KCA), focusing on its application in electricity production conditions.

Table 6. Thermodynamic performance of the Kalina cycle.

Thermodynamic Parameters	Values
Specific Work [kJ/kg]	367.66
Net Mechanical Power [kW]	2817.83
Net Electrical Power [kWe]	2565.03
Thermal Efficiency [%]	22.15
Exergy Efficiency [%]	45.12
Thermal Power to the DAR Cycle [kW]	7368.20

The characteristic points of the Kalina cycle can be seen in the T-S diagram in Figure 6. The concentration of NH_3 is the same at each point of the cycle.

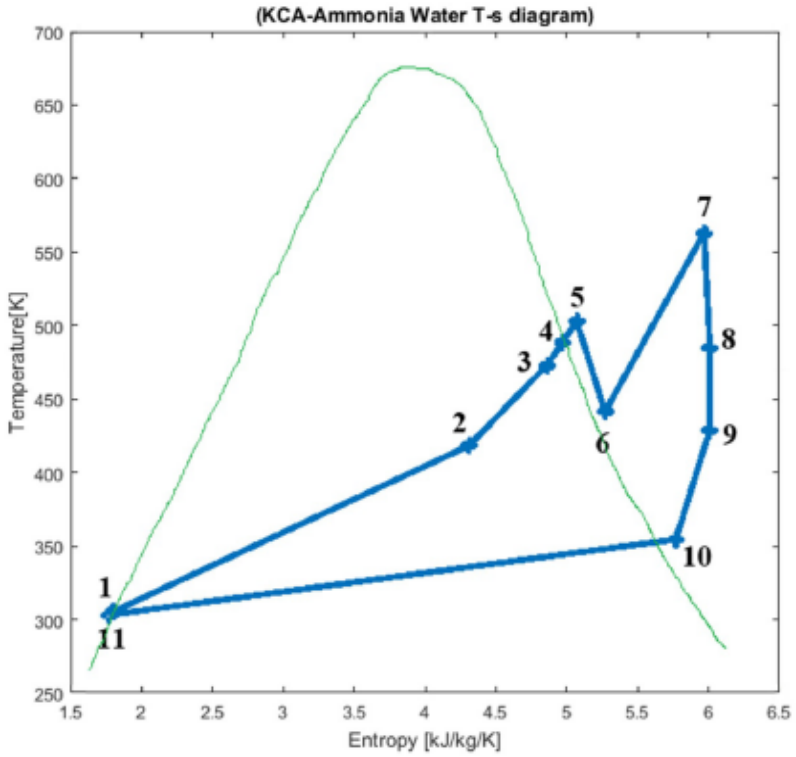

Figure 6. T-s diagrams of the Kalina cycle.

The exergy yields demonstrate a considerable improvement compared to the energy yields, as indicated in Table 7. The table displays the exergy destruction for each component under specific conditions, including a given evaporation pressure and an ammonia mass fraction of 0.88 in the working fluid.

Table 7. Exergy analysis of the components in the Kalina cycle.

Components	Exergy Destruction [kW]	Exergy Efficiency [%]
Preheater	2637.58	84.59
Evaporator	758.72	50.91
Superheater 1	790.32	65.68
Superheater 2	5086.29	64.55
HPT	1159.70	53.70
MPT	1745.38	35.69
LPT	509.47	20
Heat Exchanger 2	3261.88	79.85
Condenser	5332.39	21.72
Feed Pump 2	29.34	29.88
Feed Pump 1	8.83	88.69
Heat Exchanger 1	7456.85	89.86

Figure 7 shows the share of each component in the overall exergy destroyed in the Kalina cycle. Examining the results, Figure 7 highlights that the highest exergy destruction in the Kalina cycle system occurs in heat exchanger 1 (26%), followed by superheater 2 and the condenser (18%).

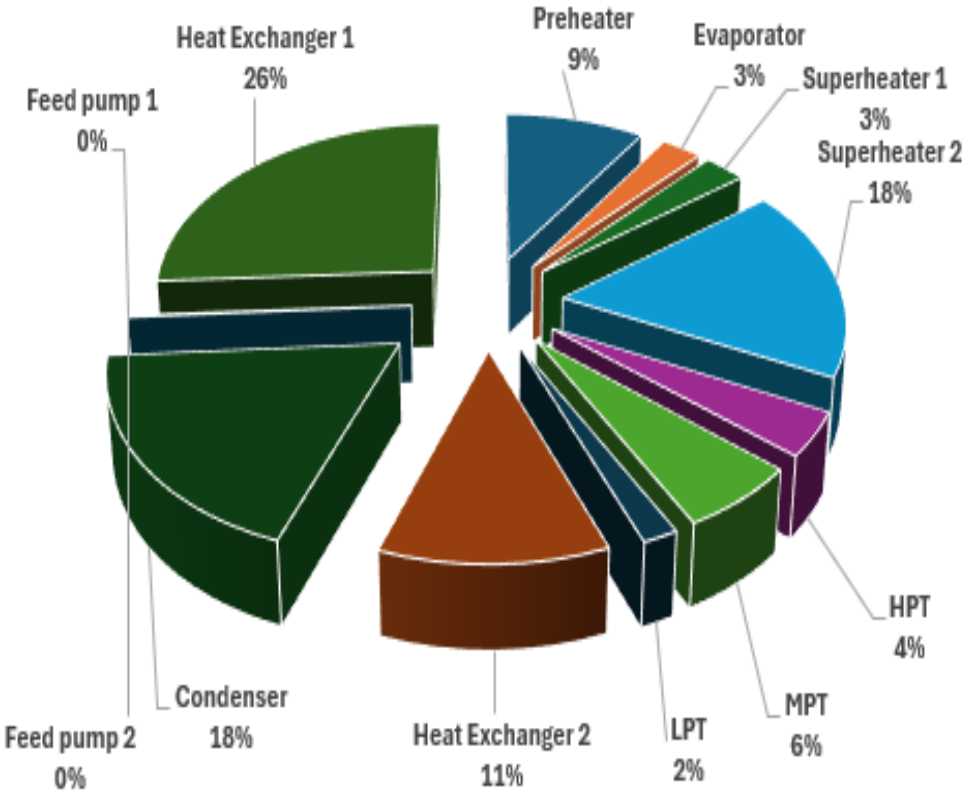

Figure 7. Exergy destruction rate of the different components of the Kalina cycle.

5.2.2. Sensitivity of the Kalina Cycle

The impact of the temperature variation at point 5 on the thermodynamic performance of the cycle is presented in Figure 8. The sensitivity study was carried out for temperatures ranging from 200 °C to 360 °C, with a temperature step of 20 °C. Figure 8 shows the variations in specific work, electrical power, mechanical power, and thermal efficiency

in response to the temperature changes in point 5. The observed trend indicates a direct proportionality between the performance parameters and the high-pressure turbine inlet temperature—higher temperatures correspond to increased values in these parameters.

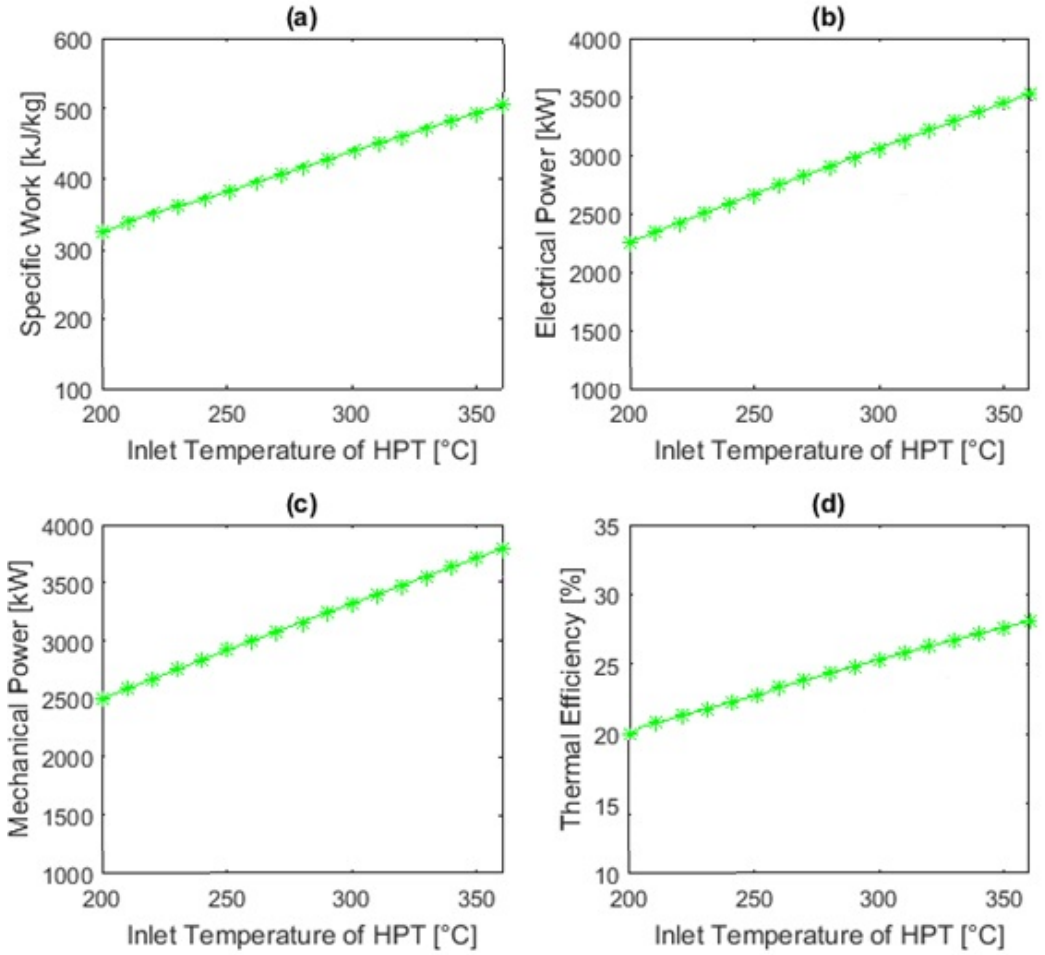

Figure 8. Influence of HPT's temperature on performance parameters.

The impact of the pressure variation, under the conditions of no variation in the ammonia mass fraction, on the thermodynamic parameters of the Kalina system is presented in Figure 9. In Figure 9a, the specific work increases considerably between 3 and 11 MPa. Between 11 and 19 MPa, the specific work is reduced. This phenomenon can also be observed in the electrical and mechanical power curves (see Figure 9b,c). Like specific work, there is a peak in electrical power with increasing pressure at approximately 12 MPa before decreasing. The same observations are true for the Kalina cycle's mechanical power and thermal efficiency.

Figure 10 shows the impact of varying the ammonia concentration on KCA performance parameters for concentrations between 60% and 94%. Increasing the ammonia concentration also leads to an increase in specific work because higher concentrations improve the thermal efficiency of the evaporator (see Figure 10a). It is worth noting that there is a slight slope in the variation in specific work with respect to ammonia concentration.

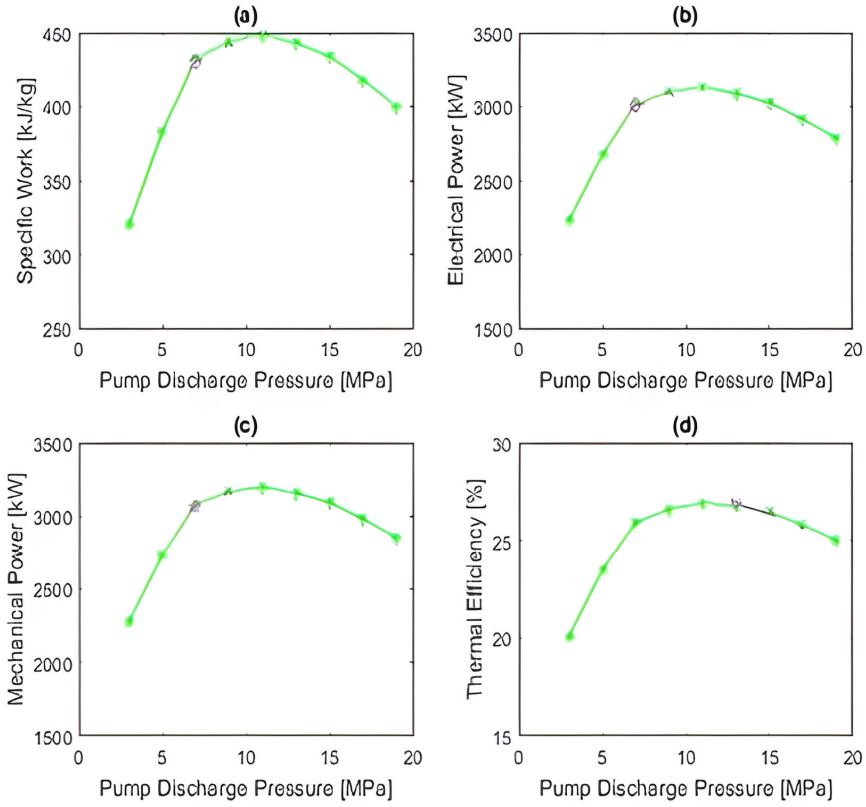

Figure 9. Influence of pump discharge pressure on performance parameters.

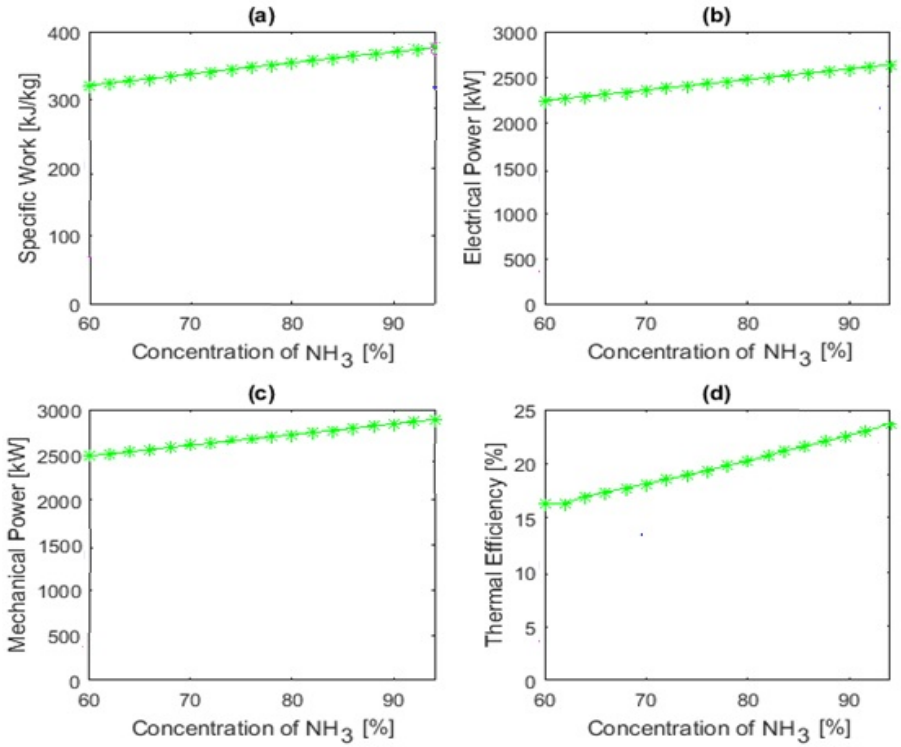

Figure 10. Influence of NH_3 concentration on performance parameters.

Figure 10b,c show the electrical and mechanical power variations with the NH_3 concentration, respectively. These figures show that, under optimal pressure conditions, the increase in concentration is also accompanied by increases in electrical and mechanical powers. The increase in power in the cycle is the increase in mass flow, which is influenced

by the variation in the NH_3 concentration. These conditions occur because there is an increased production of steam, given the richness of the mixture present.

Figure 10d shows the impact of variation in the concentration of NH_3 on thermal efficiencies. Compared to the other three variations, the slope of the increase in thermal efficiency is higher.

5.3. DAR Cycle System

5.3.1. Thermodynamic Performance

The thermodynamic performance of the DAR cycle is primarily grounded in the two laws of thermodynamics, which articulate the quantitative conservation of energy and the qualitative degradation of energy, respectively. An energy analysis of a system involves tracking the energy supplied and released by the system. The concept of exergy balance is rooted in both the laws of thermodynamics. This article's energy performance considerations encompass the cycle performance coefficient, evaporation temperature, and cooling capacity. Other heat exchanges can also be scrutinized to assess the performance of a diffusion–absorption refrigeration (DAR) machine cycle. The exergy analysis employed in this study seeks to ascertain the exergy destructions in each component of DAR and identify the elements that have a significant share in the overall destroyed exergy. Utilizing the heat flux of 7368.20 kW (at 109.5 °C) rejected by the Kalina cycle system (refer to Table 6) facilitated the derivation of the following results (as presented in Table 8 below):

Table 8. Performance study parameters of the DAR system.

Operating Parameters	Values
Heat transfer from Evaporator [kW]	6766.023
Heat transfer from Condenser [kW]	8464.306
Heat transfer from Absorber [kW]	26,322.392
Heat transfer from Generator [kW]	25,226.022
Heat transfer from Rectifier [kW]	5743.233
Coefficient of Performance [-]	0.268
Evaporator Temperature [°C]	10.57

The distribution of the different heat exchanges of the DAR components is shown in Figure 11. The absorber evacuates most of the heat exchanged (37%), followed by the generator (35%). The rest is shared almost equally between the condenser, the rectifier, and the evaporator. The less energy destruction there is, the better the coefficient of performance (COP). Table 9 shows the characteristics of the different points in the DAR cycle, while Table 10 gives the results of the exergy analysis of the DAR cycle.

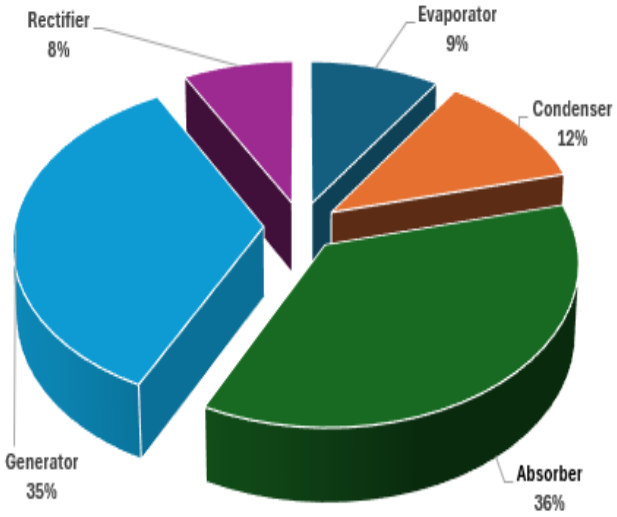

Figure 11. Distribution of heat exchanges of DAR cycle.

Table 9. Thermodynamic parameters of DAR system.

State Point	Mass Flux [kg/s]	Temperature [°C]	Pressure [bar]	Enthalpy [kJ/kg]	xNH_3 [%]	xH_2O [%]	xH_2 [%]
12	22.32	93.6	20	1303	0.9652248	0.0347752	0
13	15.21	83.6	20	860	0.0347752	0.97317555	0
14	6.94	83.6	20	1480	0.97317555	0.02682445	0
15	6.94	40.72	20	259.78	0.97317555	0.02682445	0
16	6.94	5.72	20	1480	0.97317555	0.02682445	0
17	14.47	−9.28	20	2594	0.045405	0	0.954595
18	14.47	25.72	20	2594	0.045405	0	0.954595
19	7.36	26.63	20	2778	2.314×10^{-5}	3.4066×10^{-8}	0.99997683
20	7.36	1.49	20	2788	2.314×10^{-5}	3.4066×10^{-8}	0.99997683
21	22.32	13.46	20	173	0.58182	0.41818	0
22	22.32	77.06	20	173	0.58182	0.41818	0
23	15.21	104.32	20	860	0.0347752	0.97317555	0
24	15.21	40.72	20	860	0.0347752	0.97317555	0

Table 10. Exergy efficiency and exergy destroyed in the DAR cycle.

Components	Exergy Destroyed [kW]	Exergy Efficiency [%]
Bubble Pump	18,618.06	3.28
Rectifier	4152.44	3.45
Condenser	16,987.36	28.94
GHX Exchanger	12,174.98	54.99
Evaporator	1314.92	28.43
Absorber	2177.83	15.50
SHX Exchanger	17,017.18	15.84

Figure 12 above shows that the most significant exergy destroyed is at the generator, then from the condenser, SHX, and GHX. The evaporator has low exergy destroyed, estimated at 2% of the overall exergy destruction.

5.3.2. Sensitivity of the DAR System

The influence of the generator temperature variation on the DAR cycle system is examined in Figure 13. The discharge temperature of the hot gases from the Kalina cycle is employed to study the behavior of the DAR cycle as it undergoes variations. The study spans temperatures from 100 °C to 250 °C, with a step of 10 °C. Figure 13a illustrates the evolution of the coefficient of performance (COP) with the generator temperature. The COP increases until 150 °C and then decreases with temperature increase toward 250 °C. The optimal COP value is observed at a temperature of 150 °C. Figure 13a indicates that high temperatures alone are insufficient for achieving good COPs. Since the COP is a function of the evaporator power, the same holds for the variation in the evaporator power with the generator temperature (Figure 13c). As the operating temperature increases under constant pressure conditions, the Qevap (directly proportional to COP) has a maximum value at the optimum temperature. After the optimum point, the Qevap decreases as the

temperature increases, as shown in Figure 13c. This situation can also be observed in the cases of Figure 14b,d.

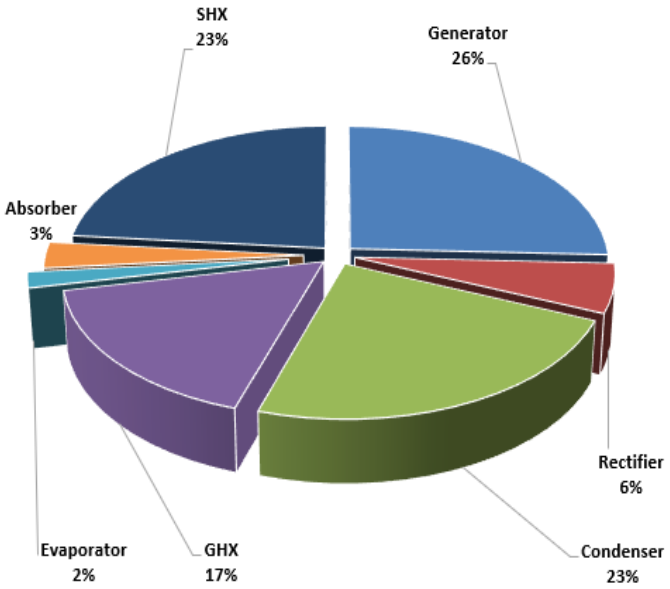

Figure 12. Distribution of exergy destroyed in the different organs of the DAR.

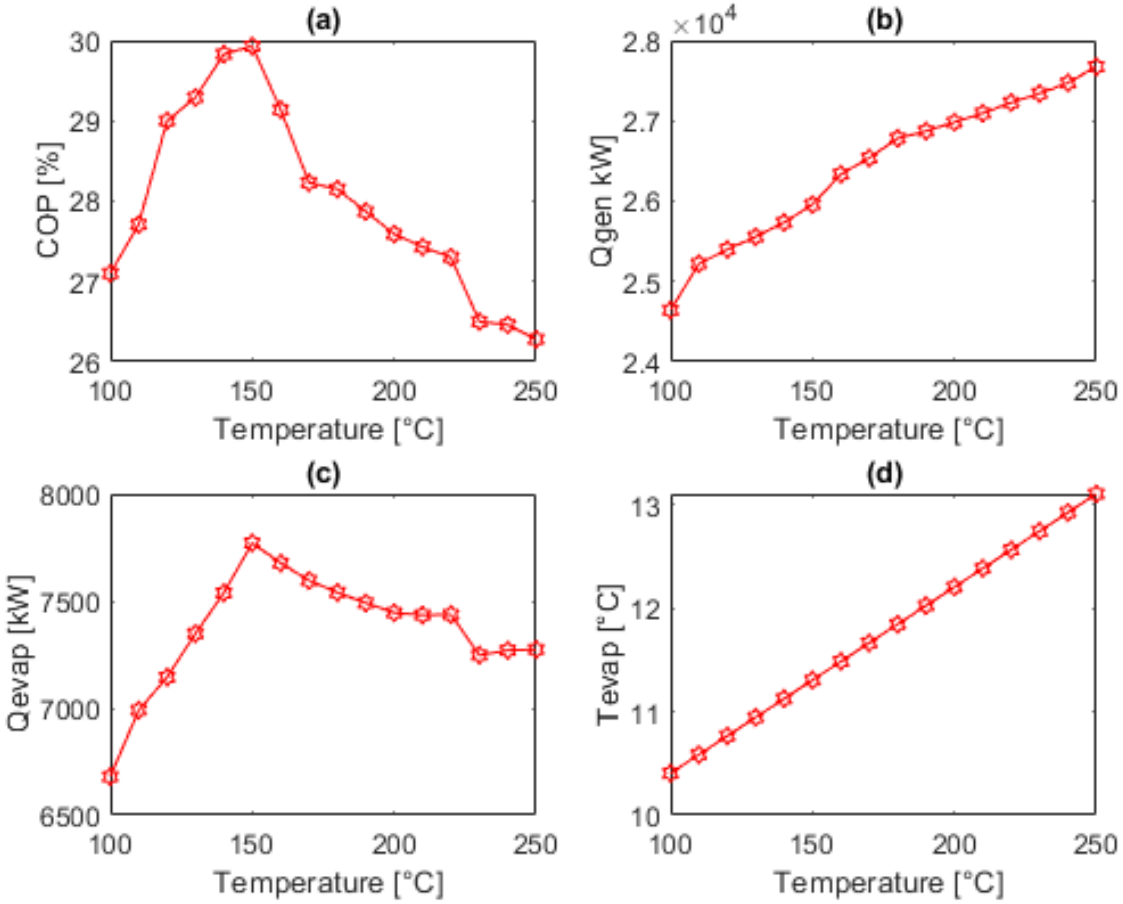

Figure 13. Influence of the generator's temperature variation on the (**a**) coefficient of performance, (**b**) generator power, (**c**) evaporator power, and (**d**) temperature of the evaporator.

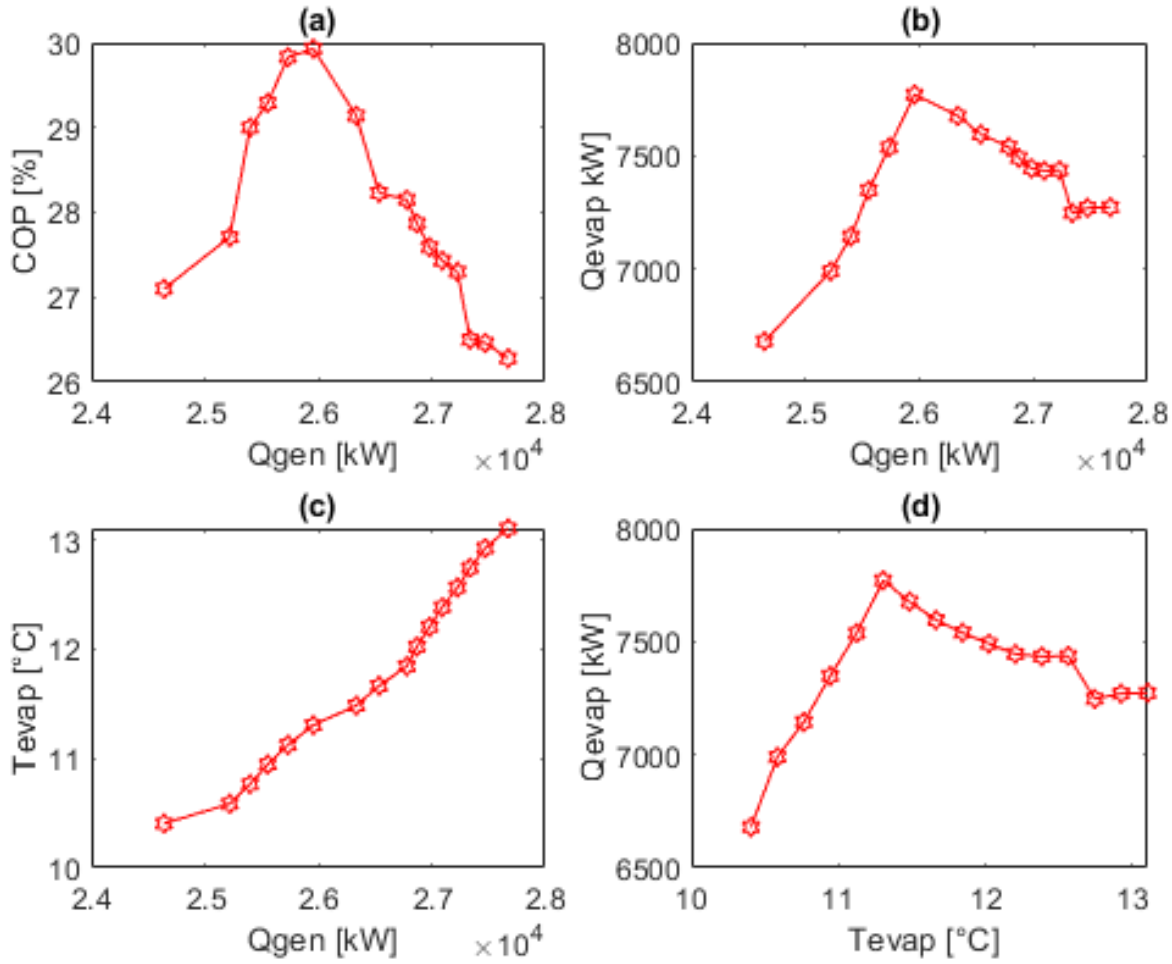

Figure 14. Sensibility to the generator power (under the effect of the generator's temperature variation) of the (**a**) coefficient of performance, (**b**) evaporator power, (**c**) temperature of the evaporator, and (**d**) sensibility of the evaporator power to the temperature of the evaporator (under the effect of the generator's temperature variation).

Figure 13b depicts the variation in generator power with the generator temperature. This curve is not linear due to the instabilities observed, particularly in the flow rates of hot gases and the water–ammonia solution. The curve in Figure 13d shows the ascending linear relationship between the evaporator and generator temperatures. Unlike COP, the evaporator temperature increases with the generator temperature throughout the variation, indicating a proportional relationship between the two variables.

Figure 14 illustrates the variation in different parameters with the generator's power. The generator's power varies with the generator's temperature, such that each point in Figure 14 corresponds to a temperature between 100 to 250 °C. The COP variation with the generator's power illustrated in Figure 14a behaves as with temperature in Figure 13a; the COP increases with the generator's power up to a power of approximately 2.6×10^4 kW. At higher powers, the COP decreases. Figure 14a indeed validates the relationship, making it possible to calculate COP as a function of both temperature and power. Figure 14b, for its part, is also like the curve in Figure 13c, allowing us to notice a similar influence of the temperature and generator power on the variation in the cooling power. An evaporator power peak is observed when the generator power indicates the value of 2.6×10^4 kW. The relationship between the evaporator temperature and generator power is illustrated in Figure 14c, which shows a quasi-linear ascending curve. As the generator power increases, the evaporator temperature also increases. Figure 14d illustrates the relationship between

the evaporator temperature and power. This curve behaves similarly to those in Figure 13c. The reason is that T_{evap} is directly proportional to T_{gen} and Q_{gen}.

As in Figure 13a, the peak in Figure 14a shows that for a given absorber efficiency of 0.8 and an evaporation temperature of 10.57 °C, the COP increases sharply up to a particular maximum value, then gradually decreases as the generation temperature (or generation power) increases.

The sensitivity of the circuit to the pressure variation in the DAR cycle system is shown in Figure 15. The evolution of COP with the pressure variation is shown in Figure 15a. The latter shows that an increase in COP accompanies the increase in pressure. Figure 15b shows that the generator's power is inversely proportional to the pressure; Q_{gen} decreases as pressure increases. Figure 15c highlights the variation in the evaporator power with the circuit pressure. The two variables are directly proportional. And finally, Figure 15d represents the evolution of T_{evap} as a function of the pressure variation. The evaporation temperature decreases with increasing pressure.

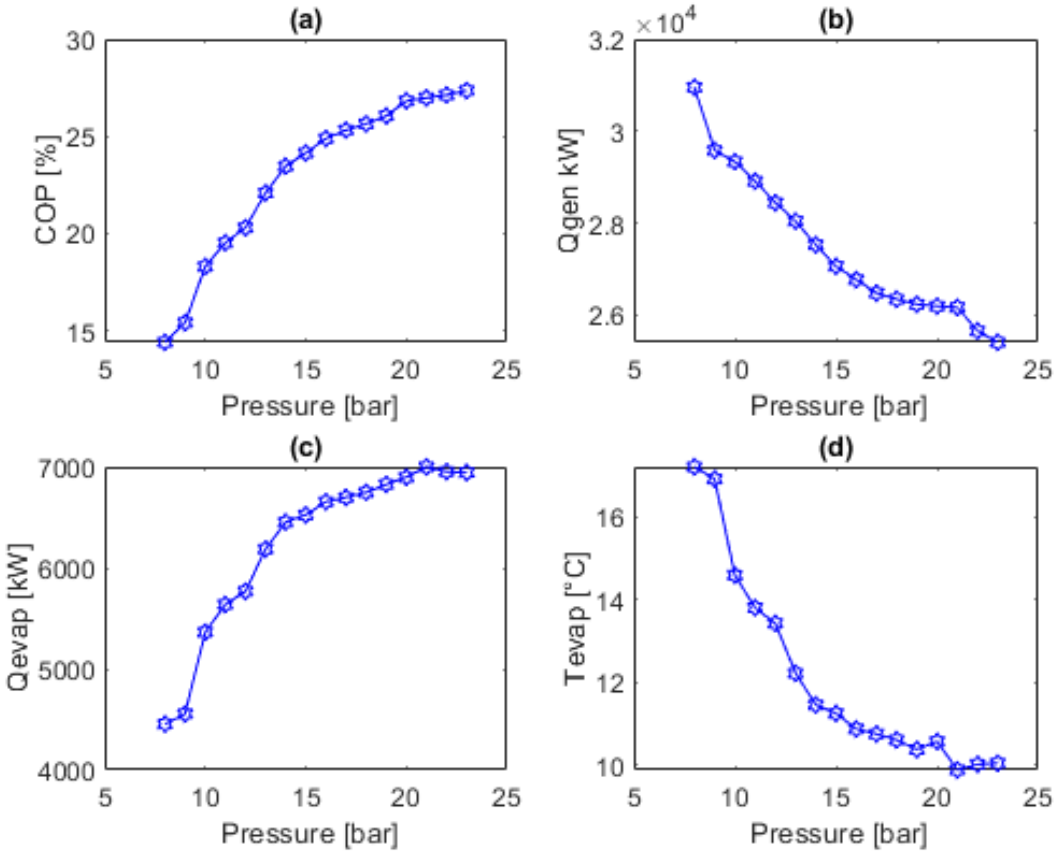

Figure 15. Sensibility to the cycle pressure variation of the (**a**) coefficient of performance, (**b**) generator power, (**c**) evaporator power, and (**d**) temperature of the evaporator.

Figure 16 illustrates the performance variation with the generator power associated with a range of pressure variations from 8 to 23 bars, incremented by 1 bar. Each point on these graphs represents a specific pressure value. Figure 16a shows the variations in the coefficient of performance with the generator's power when the pressure varies. The COP has its optimal values only at low Q_{gen} values. Similarly, Figure 16b demonstrates a decrease in Q_{evap} as Q_{gen} increases. Figure 16c is essentially the mirrored image of Figure 16a. T_{evap} is almost constant, then increases, with variable slopes until the Q_{gen} values close to 2.9 kW. Beyond this point, the slope diminishes considerably. When the pressure fluctuates, the cooling capacity decreases as T_{evap} increases, as depicted in Figure 16d.

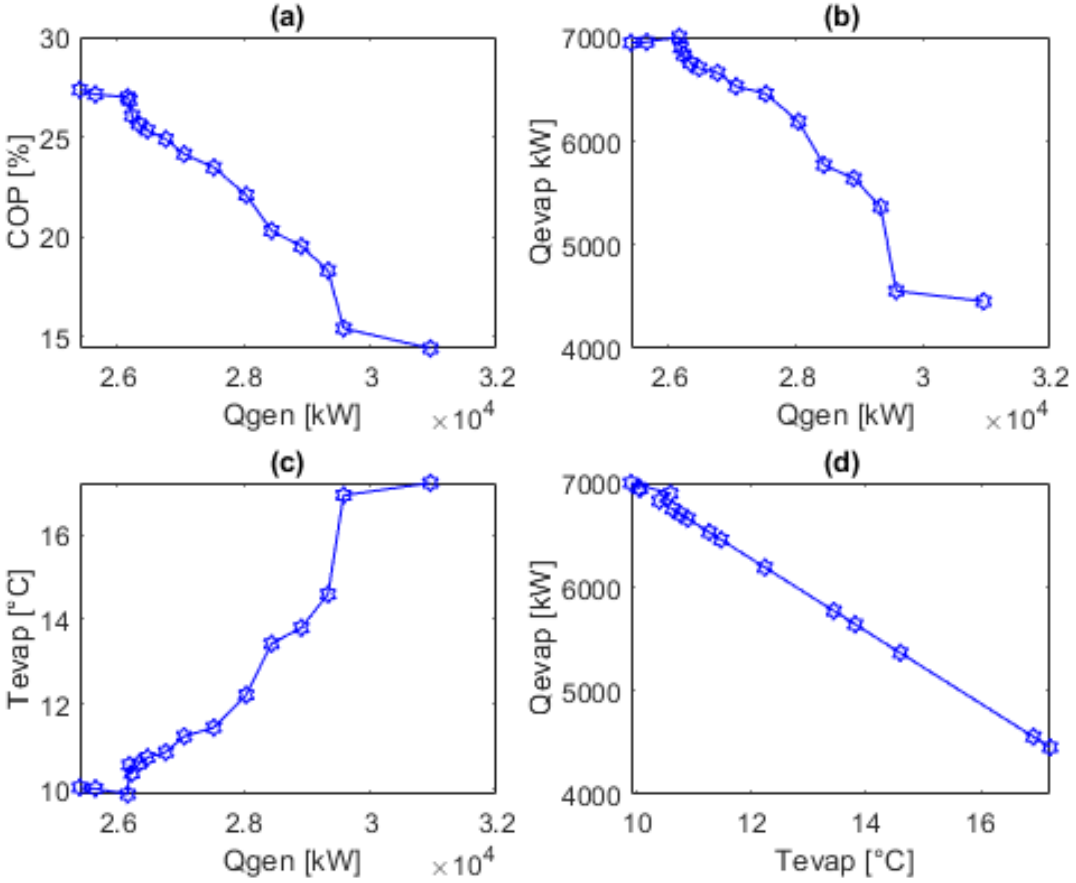

Figure 16. Sensibility to the generator power (under the effect of the cycle's pressure variation) of the (**a**) coefficient of performance, (**b**) evaporator power, (**c**) temperature of the evaporator, and (**d**) sensibility to the temperature of the evaporator (under the effect of the cycle's pressure variation) of the evaporator power.

5.4. Domestic Hot Water System

In the domestic heating network standard, orders of magnitude (set temperatures) are recommended for reaching or approaching. The set temperatures considered sufficient are as follows (https://energieplus-lesite.be/, accessed on 27 December 2023): body care, approximately 45 °C; collective shower, around 40 °C; domestic kitchen, around 50 °C; professional kitchen, around 60 °C, and disinfection (butchery), up to 90 °C. In this work, the water's final temperature, after heat exchange with the residual gases at $T_{rej2} = 45.9$ °C, is $T_{HW} = 42.72$ °C. The thermal efficiency reaches 27.71%. Regarding the setpoint temperatures mentioned above, the hot water temperature found in the present work falls within the range of setpoint values, i.e., 40 to 50 °C (for the case of residential houses).

5.5. Biogas Production System

The biogas production discussed in this article is mesophilic, given that the temperature level released by the domestic hot water system is 33.18 °C. The waste is of the agricultural biomass type, with a lower calorific value of 17.2 MJ/kg [47] and a specific heat of 1332 kJ/kg/K. Using the residual gases leaving the domestic hot water heating, the heat exchanger increases the sensible heat per unit of time (thermal power) of the biomass in the biodigester from 195.24 MW to 206.75 MW and accelerates biogas production. Figure 17 illustrates the influence of the residual heat of the gases on the biomass contained in the biodigester.

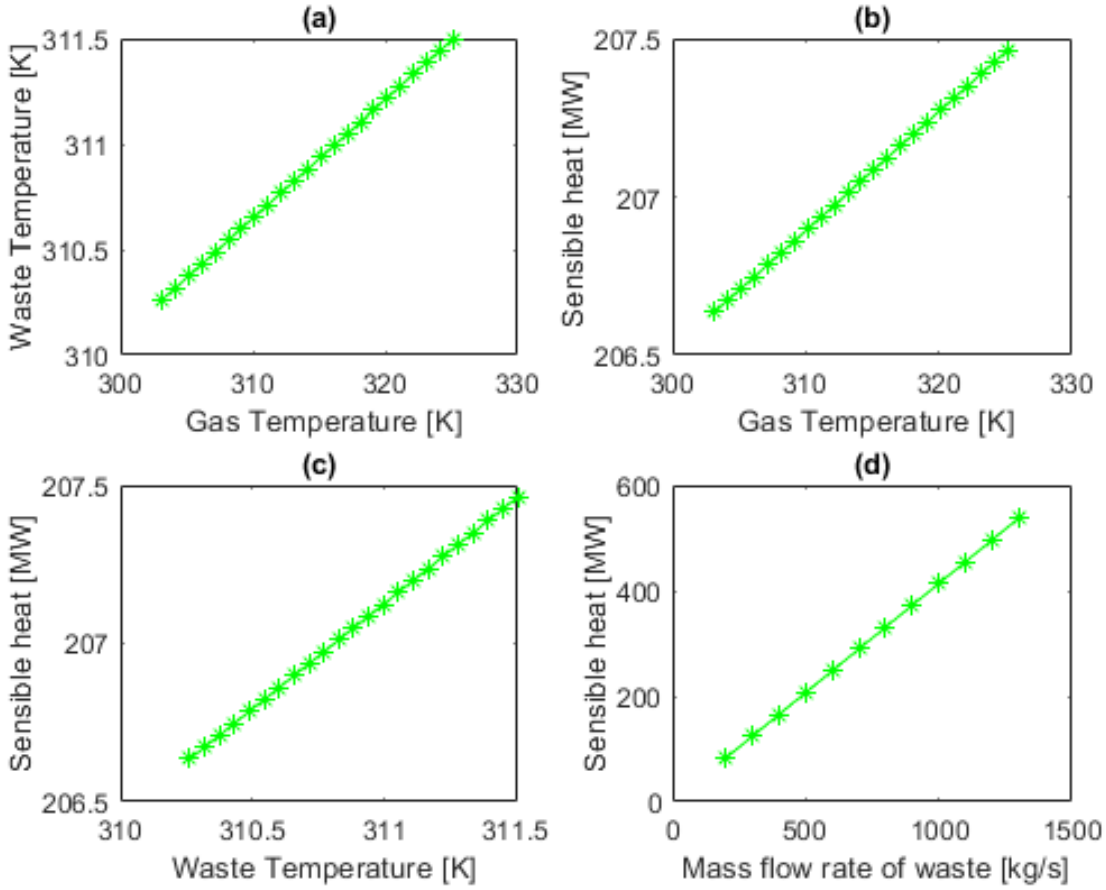

Figure 17. Variation in biomass properties according to gases' residual heat characteristics.

Figure 17a,b, respectively, represent the effect of the variation in gas temperature on the waste temperature and the sensible heat per unit of time (thermal power) of the waste. Figure 17c relates the waste's temperature and the waste's thermal power (sensible heat per unit of time) after heat exchange with the hot gases when the gas temperature varies. Finally, Figure 17d represents the effect of the variation in the waste's mass flow rate on the waste's sensible heat per unit of time after heat exchange with the hot gases.

6. Conclusions and Perspectives

In this study, the thermal performance and energy and exergy conservation in Kalina cycle and DAR cycle systems using H_2O+NH_3 and H_2O+NH_3+H_2 as working fluids, respectively, are investigated. In the first part of the study, the Kalina cycle is coupled with the circuit of hot gases leaving the rotating cement kiln via a water circuit. And the second part of this study brings together the diffusion–absorption refrigeration machine cycle (DAR), the domestic hot water circuit, and residual heat to produce biogas. The major conclusions are listed as follows:

- The three turbines and two superheaters in the Kalina cycle are intended to make the system efficient.
- The energy in the hot gases was recovered in two places: the hot gases exiting the preheating tower and those exiting the clinker cooler.
- The Kalina cycle system aims to produce electricity, thanks to the recovery of the energy in the gases leaving the rotary kiln. The Kalina cycle gives an electrical power of 2565.03 kWe. The efficiencies of the two laws of thermodynamics are 22.15% and 45.12%, respectively, thermal efficiency and exergy efficiency. The model gives satisfactory results in the different sensitivity cases studied.

- The DAR cycle aims to produce cold using the energy of the gases leaving the Kalina cycle circuit.
- The gas energy rejected by the DAR cycle is used to heat domestic hot water and waste in a biodigester.
- In the case of the DAR cycle, a coefficient of performance of 0.268, an evaporation temperature of 10.57 °C, and a refrigeration capacity of 6766.023 kW were found. The study of the model's sensitivity to generator temperature and pressure variations also gave good results. In the case of a water heating network, the hot water temperature found in the present work falls within the range of setpoint values, i.e., 40 to 50 °C (for the case of residential houses).
- In the biogas production circuit, the waste sensible heat per unit of time (thermal power), after heat exchange with the hot gases, amounts to 206.75 MW for a flow rate of 500 kg/s.
- The results of the different sub-models of this article were the subject of a comparison and validation study with data from the literature. This study, therefore, validated all the sub-models. Although the proposed multigeneration system gives promising results, it is important to analyze its critical parameters while reducing the assumptions and recalculating the optimal system parameters.

Author Contributions: Conceptualization, B.-J.R.M.B., R.M., M.T.M. and A.I.; Methodology, B.-J.R.M.B., R.M., M.T.M. and A.I.; Software, B.-J.R.M.B., M.T.M. and L.M.M.; Validation, B.-J.R.M.B. and A.I.; Formal analysis, B.-J.R.M.B., R.M., M.T.M., L.M.M. and A.I.; Investigation, B.-J.R.M.B., M.T.M., L.M.M. and A.I.; Resources, B.-J.R.M.B.; Data curation, B.-J.R.M.B., R.M., M.T.M. and L.M.M.; Writing—original draft, B.-J.R.M.B.; Writing—review & editing, B.-J.R.M.B. and A.I.; Visualization, R.M., M.T.M. and L.M.M.; Supervision, A.I.; Project administration, B.-J.R.M.B. and A.I.; Funding acquisition, A.I. All authors have read and agreed to the published version of the manuscript.

Funding: The postdoctoral research was funded by the Futuris Research Institute (InReF) of the Democratic Republic of Congo. The APC was funded by the École de Technologie Supérieure, Université du Québec. Discovery research grant RGPIN-2019-04220 is from NSERC support.

Data Availability Statement: The original contributions presented in the study are included in the article, further inquiries can be directed to the corresponding author.

Acknowledgments: The authors thank the Futuris Research Institute (InReF) of the Democratic Republic of Congo for scientific collaboration.

Conflicts of Interest: The authors declare that they have no known competing financial interests or personal relationships that could have appeared to influence the work reported in this paper.

List of Abbreviations and Symbols

Latin Letters

Symbol	Signification	Unit
A	Heat Transfer Surface area	m^2
$\dot{Ex}$	Primary exergy	kJ
ex	Specific exergy	kJ/kg
F_i	Dimensional factor	-
h	Specific enthalpy	kJ/kg
h_i	Global coefficient of heat transfers	$kW/m^2/K$
$\dot{m}$	Mass flow rate	kg/s
$\dot{Q}$	Thermal power	kW
$\dot{q}_i$	Exhausted gas heat transfer rate	kW
s	Specific entropy	kJ/kg/K
T	Temperature	K
T_{gsor}	Exit gas temperature	K
ΔT	Variation in temperature	K
$\dot{w}$	Work per time unit	kJ/s
x_{NH3}	NH_3 concentration in the mixture	%

Greek Letters

η	Efficiency	%
ε	Efficiency	%

Subscripts

abs	Absorber
amb	Ambient
BGP	Biogas production
cond	Condenser
evap	Evaporator
gcol	Gas from cooler
*gcol*1	Exit gas from cooler before heat exchanger 2
*gcol*2	Exit gas from cooler after heat exchanger 2
gcy	Exit gas from cyclone
*gcy*1	Exit gas from cyclone before heat exchanger 1
*gcy*2	Exit gas from cyclone after heat exchanger 1
gen	Generator
GHX	Gas heat exchanger
*HEX*1	Heat exchanger 1
*HEX*2	Heat exchanger 2
HExW	Heat exchanger of hot water
HR	Potential amount of heat recovery from this process
*HR*1	Recovery of heat 1
*HR*2	Recovery of heat 2
HW	Hot water
HWT	Hot water tank
*HWT*2	Hot water tank 2
In	Inlet
isHPT	Isentropic, high-pressure turbine
isLPT	Isentropic, low-pressure turbine
isPump	Isentropic, pump
LMTD	Due to the Logarithmic Mean Temperature Difference
Out	Outlet
P	Pump
preh	Preheater
*pump*1	Feed pump 1
*pump*2	Feed pump 2
Rec	Heat recovered amount in the regenerator
rec	Rectifier
*rej*2	Rejected (gas rejected from the DAR cycle)
*rej*3	Rejected (gas rejected from the domestic hot water)
SHX	Solution heat exchanger
*superh*1	Superheater 1
*superh*2	Superheater 2
T	Turbine
Waste	Solid waste
waste, 1	Solid waste before heat exchanger with hat gas
waste, 2	Solid waste after heat exchanger with hat gas
0	Environmental condition.

Superscripts

D	Concerned exergy destroyed
Q	Refers to heat transfer
W	Refers to power

Abbreviations

DAR	Diffusion–absorption refrigerant
GHX	Gas heat exchanger
HPT	High-pressure turbine
IEA	International Energy Agency
KCA	Kalina cycle (A)
LNG	Liquefied natural gas
LPT	Low-pressure turbine
MPT	Medium-pressure turbine
ORC	Organic Rankine cycle
RDF	Refuse-derived fuel
SHX	Solution heat exchanger

References

1. Mollahosseini, A.; Abdelrasoul, A.; Sheibany, S.; Amini, M.; Salestan, S.K. Renewable Energy-Driven Desalination Opportunities—A Case Study. *J. Environ. Manag.* **2019**, *239*, 187–197. [CrossRef] [PubMed]
2. Ghasemiasl, R.; Khalili Abhari, M.; Javadi, M.A.; Ghomashi, H. 4E Investigating of a Combined Power Plant and Converting It to a Multigeneration System to Reduce Environmental Pollutant Production and Sustainable Development. *Energy Convers. Manag.* **2021**, *245*, 114468. [CrossRef]
3. Júnior, E.P.B.; Arrieta, M.D.P.; Arrieta, F.R.P.; Silva, C.H.F. Assessment of a Kalina Cycle for Waste Heat Recovery in the Cement Industry. *Appl. Therm. Eng.* **2019**, *147*, 421–437. [CrossRef]
4. Varma, G.V.P.; Srinivas, T. Parametric Analysis of Steam Flashing in a Power Plant Using Waste Heat of Cement Factory. *Energy Procedia* **2016**, *90*, 99–106. [CrossRef]
5. Cheng, Z.; Wang, J.; Yang, P.; Wang, Y.; Chen, G.; Zhao, P.; Dai, Y. Comparison of Control Strategies and Dynamic Behaviour Analysis of a Kalina Cycle Driven by a Low-Grade Heat Source. *Energy* **2022**, *242*, 122958. [CrossRef]
6. Hossain, M.M.; Hossain, M.S.; Ahmed, N.A.; Ehsan, M.M. Numerical Investigation of a Modified Kalina Cycle System for High-Temperature Application and Genetic Algorithm Based Optimization of the Multi-Phase Expander's Inlet Condition. *Energy AI* **2021**, *6*, 100117. [CrossRef]
7. Kumar Singh, S.; Kumar Tiwari, A.; Paliwal, H.K. Techno-Economic Assessment of Retrofitted Parabolic Trough Collector for Kalina Power Cycle. *Appl. Therm. Eng.* **2024**, *236*, 121550. [CrossRef]
8. da Costa Horta, G.R.; Barbosa, E.P.; Moreira, L.F.; Arrieta, F.R.P.; de Oliveira, R.N. Comparison of Kalina Cycles for Heat Recovery Application in Cement Industry. *Appl. Therm. Eng.* **2021**, *195*, 117167. [CrossRef]
9. Ma, H.; Xie, Y.; Duan, K.; Song, X.; Ding, R.; Hou, C. Dynamic Control Method of Flue Gas Heat Transfer System in the Waste Heat Recovery Process. *Energy* **2022**, *259*, 125010. [CrossRef]
10. Zhao, X.; Chen, H.; Li, S.; Li, W.; Pan, P.; Liu, T.; Wu, L.; Xu, G. Thermodynamic and Economic Analysis of a Novel Design Combining Waste Tire Pyrolysis with Silicon Production Waste Heat Recovery and Organic Rankine Cycle. *Energy* **2023**, *283*, 128500. [CrossRef]
11. Cao, Y.; Zhan, J.; Jia, B.; Chen, R.; Si, F. Optimum Design of Bivariate Operation Strategy for a Supercritical/Transcritical CO_2 Hybrid Waste Heat Recovery System Driven by Gas Turbine Exhaust. *Energy* **2023**, *284*, 129325. [CrossRef]
12. Zhang, G.; Zhang, S.; Sun, B.; Liu, J.; Yan, J. Design on a Novel Waste Heat Recovery System Integrated with the Bypass Flue and Outside Primary Air Preheater for Bitumite-Fired Power Plants. *Energy* **2024**, *291*, 130341. [CrossRef]
13. Fu, B.-R.; Hsieh, J.-C.; Cheng, S.-M.; Royandi, M.A. Thermoeconomic Analysis of a Novel Cogeneration System for Cascade Recovery of Waste Heat from Exhaust Flue Gases. *Appl. Therm. Eng.* **2024**, *247*, 123034. [CrossRef]
14. Feng, J.; Cheng, X.; Wang, H.; Zhao, L.; Dong, H. Effect of Flue Gas Outlet Temperature in Evaporator on Thermal Economic Performance of Organic Rankine Cycle System for Sinter Waste Heat Recovery. *J. Iron Steel Res. Int.* **2023**, *30*, 2378–2390. [CrossRef]
15. Wang, Q.; Macián-Juan, R.; Li, D. Analysis and Assessment of a Novel Organic Flash Rankine Cycle (OFRC) System for Low-temperature Heat Recovery. *Energy Sci. Eng.* **2022**, *10*, 3023–3043. [CrossRef]
16. Benvenuto, G.; Trucco, A.; Campora, U. Optimization of Waste Heat Recovery from the Exhaust Gas of Marine Diesel Engines. *Proc. Inst. Mech. Eng. Part M J. Eng. Marit. Environ.* **2016**, *230*, 83–94. [CrossRef]
17. Liang, Y.; Chen, W.; Luo, X.; Chen, J.; Yang, Z.; Chen, Y. Multi-Objective Optimization of Supercritical CO_2 Brayton Cycles for Coal-Fired Power Generation with Two Waste Heat Recovery Schemes. *Energy Convers. Manag.* **2024**, *300*, 117962. [CrossRef]
18. Zhu, Y.; Li, J.; Ge, M.; Gu, H.; Wang, S. Numerical and Experimental Study of a Non-Frosting Thermoelectric Generation Device for Low Temperature Waste Heat Recovery. *Appl. Energy* **2023**, *352*, 121952. [CrossRef]
19. Adjibade, M.I.S.; Thiam, A.; Awanto, C.; Azilinon, D. Experimental Analysis of Diffusion Absorption Refrigerator Driven by Electrical Heater and Engine Exhaust Gas. *Case Stud. Therm. Eng.* **2017**, *10*, 255–261. [CrossRef]

20. Karamangil, M.I.; Coskun, S.; Kaynakli, O.; Yamankaradeniz, N. A Simulation Study of Performance Evaluation of Single-Stage Absorption Refrigeration System Using Conventional Working Fluids and Alternatives. *Renew. Sustain. Energy Rev.* **2010**, *14*, 1969–1978. [CrossRef]
21. Starace, G.; De Pascalis, L. An Enhanced Model for the Design of Diffusion Absorption Refrigerators. *Int. J. Refrig.* **2013**, *36*, 1495–1503. [CrossRef]
22. Zohar, A.; Jelinek, M.; Levy, A.; Borde, I. Numerical Investigation of a Diffusion Absorption Refrigeration Cycle. *Int. J. Refrig.* **2005**, *28*, 515–525. [CrossRef]
23. Chua, H.T.; Toh, H.K.; Ng, K.C. Thermodynamic Modeling of an Ammonia–Water Absorption Chiller. *Int. J. Refrig.* **2002**, *25*, 896–906. [CrossRef]
24. Mansouri, R.; Boukholda, I.; Bourouis, M.; Bellagi, A. Modelling and Testing the Performance of a Commercial Ammonia/Water Absorption Chiller Using Aspen-Plus Platform. *Energy* **2015**, *93*, 2374–2383. [CrossRef]
25. Mansouri, R.; Bourouis, M.; Bellagi, A. Steady State Investigations of a Commercial Diffusion-Absorption Refrigerator: Experimental Study and Numerical Simulations. *Appl. Therm. Eng.* **2018**, *129*, 725–734. [CrossRef]
26. Lee, G.; Choi, H.W.; Kang, Y.T. Cycle Performance Analysis and Experimental Validation of a Novel Diffusion Absorption Refrigeration System Using R600a/n-Octane. *Energy* **2021**, *217*, 119328. [CrossRef]
27. Dhindsa, G.S. Review on Performance Enhancement of Solar Absorption Refrigeration System Using Various Designs and Phase Change Materials. *Mater. Today Proc.* **2021**, *37*, 3332–3337. [CrossRef]
28. Alcântara, S.C.S.; Lima, A.A.S.; Ochoa, A.A.V.; de Leite, N.P.G.; da Costa, J.Â.P.; dos Santos, C.A.C.; Cavalcanti, E.J.C.; Michima, P.S.A. Implementation of the Characteristic Equation Method in Quasi-Dynamic Simulation of Absorption Chillers: Modeling, Validation and First Results. *Energy Convers. Manag. X* **2022**, *13*, 100165. [CrossRef]
29. Fouda, A.; Khaliq, A.; Elattar, H.F.; Al-Zahrani, A.; Almohammadi, B.A.; Refaey, H.A. Evaluation of a Concentrated Solar Power-Driven System Designed for Combined Production of Cooling and Hydrogen. *Case Stud. Therm. Eng.* **2024**, *59*, 104567. [CrossRef]
30. Almohammadi, B.A.; Al-Zahrani, A.; Refaey, H.A.; Attia, E.-A.; Fouda, A. Energy Analysis of a Novel Solar Tri-Generation System Using Different ORC Working Fluids. *Case Stud. Therm. Eng.* **2023**, *45*, 102918. [CrossRef]
31. Mazouz, S.; Mansouri, R.; Bellagi, A. Experimental and Thermodynamic Investigation of an Ammonia/Water Diffusion Absorption Machine. *Int. J. Refrig.* **2014**, *45*, 83–91. [CrossRef]
32. Cefarin, M. Design of NH3-H2O Absorption Chiller for Low Grade Waste Heat Recovery. Università degli Studi di Udine. Available online: https://core.ac.uk/download/pdf/158819668.pdf (accessed on 16 December 2023).
33. Vijayaraghavan, S. Thermodynamic Studies on Alternate Binary Working Fluid Combinations and Configurations for a Combined Power and Cooling Cycle. Ph.D. Thesis, University of Florida, Gainesville, FL, USA, 2003.
34. Aziz, M.; Juangsa, F.B.; Irhamna, A.R.; Irsyad, A.R.; Hariana, H.; Darmawan, A. Ammonia Utilization Technology for Thermal Power Generation: A Review. *J. Energy Inst.* **2023**, *111*, 101365. [CrossRef]
35. Shanmugam, S.K.G.; Mital, M. An Ultra-Low Ammonia Charge System for Industrial Refrigeration. *Int. J. Refrig.* **2019**, *107*, 344–354. [CrossRef]
36. Yamamoto, E.Y.; Leal Da Silva, R.; Higa, M. Performance Improvements on Energy and Exergy Basis for an Ammonia-Water Absorption Refrigeration System in a Coffee Industry. *Sustain. Energy Technol. Assess.* **2022**, *52*, 102284. [CrossRef]
37. Mehr, A.S.; Zare, V.; Mahmoudi, S.M.S. Standard GAX versus Hybrid GAX Absorption Refrigeration Cycle: From the View Point of Thermoeconomics. *Energy Convers. Manag.* **2013**, *76*, 68–82. [CrossRef]
38. Han, W.; Chen, Q.; Sun, L.; Ma, S.; Zhao, T.; Zheng, D.; Jin, H. Experimental Studies on a Combined Refrigeration/Power Generation System Activated by Low-Grade Heat. *Energy* **2014**, *74*, 59–66. [CrossRef]
39. SCFP L'ammoniac. Available online: https://scfp.ca/lammoniac#:~:text=L'ammoniac%20est%20corrosif%20pour,ammoniac%20lib%C3%A9r%C3%A9%20dans%20l'atmosph%C3%A8re (accessed on 16 December 2023).
40. Mungyeko Bisulandu, B.-J.R.; Ilinca, A.; Tsimba Mboko, M.; Mbozi Mbozi, L. Thermodynamic Performance of a Cogeneration Plant Driven by Waste Heat from Cement Kilns Exhaust Gases. *Energies* **2023**, *16*, 2460. [CrossRef]
41. Rattner, A.S.; Garimella, S. Low-Source-Temperature Diffusion Absorption Refrigeration. Part I: Modeling and Cycle Analysis. *Int. J. Refrig.* **2016**, *65*, 287–311. [CrossRef]
42. Rattner, A.S.; Garimella, S. Low-Source-Temperature Diffusion Absorption Refrigeration. Part II: Experiments and Model Assessment. *Int. J. Refrig.* **2016**, *65*, 312–329. [CrossRef]
43. Yousuf, N.; Biteau, E.; Anderson, T.; Gschwendtner, M.; Nates, R. Modelling the Performance of a Diffusion Absorption Refrigeration System. In Proceedings of the 2014-Asia-Pacific Solar Research Conference, Sydney, Asutralia, 8–10 December 2014.
44. Long, Z.; Luo, Y.; Li, H.; Bu, X.; Ma, W. Performance Analysis of a Diffusion Absorption Refrigeration Cycle Working with TFE–TEGDME Mixture. *Energy Build.* **2013**, *58*, 86–92. [CrossRef]
45. Hu, Z.; Deng, Z.; Gao, W.; Chen, Y. Experimental Study of the Absorption Refrigeration Using Ocean Thermal Energy and Its Under-Lying Prospects. *Renew. Energy* **2023**, *213*, 47–62. [CrossRef]

46. Mansouri, R.; Bourouis, M.; Bellagi, A. Experimental Investigations and Modelling of a Small Capacity Diffusion-Absorption Refrigerator in Dynamic Mode. *Appl. Therm. Eng.* **2017**, *113*, 653–662. [CrossRef]
47. Mungyeko Bisulandu, B.-J.R.; Marias, F. Numerical Modeling of Thermochemical Conversion of Biomass and Tires as Fuels for Cement Clinker Production. *Recycling* **2023**, *8*, 41. [CrossRef]